Delayed activation of the DNA replication licensing system in Lgr5(+) intestinal stem cells

T.D. Carroll[1], I.P. Newton[1], J.J. Blow*[2], I.Näthke*[1]

Affiliations: [1]Cell & Developmental Biology and [2]Centre for Gene Regulation and Expression, University of Dundee, Dundee, Scotland, UK, DD15EH
*Correspondence to: j.j.blow@dundee.ac.uk or i.s.nathke@dundee.ac.uk

ABSTRACT

During late mitosis and early G_1, replication origins are licensed for replication by binding to MCM2-7 double hexamers. This signals proliferative fate commitment. Here, we investigate how licensing and proliferative commitment are coupled in the small-intestinal epithelium. We developed a method for identifying cells in intestinal crypts that contain DNA-bound MCM2-7 and are licensed for replication. Interphase cells at the top of the transit amplifying zone did not contain DNA-bound MCM2-7, but still expressed MCM2-7 protein. This suggests licensing is inhibited immediately at terminal differentiation, after a final mitosis. Strikingly, we found that at the crypt base the majority of Lgr5(+) intestinal stem cells reside in an unlicensed state, despite expressing MCM2-7 protein and the Ki67 proliferation marker. This state, which we call 'shallow-G_0', might allow stem cells to be easily activated to re-enter the cell cycle. We demonstrate that the dynamics of the licensing system provides a novel means to assess the unique cell-cycle of intestinal epithelial cells.

Delayed activation of the DNA replication licensing system in Lgr5(+) intestinal stem cells

INTRODUCTION

Cell division is necessary for adult tissue homeostasis. It allows for the replacement of aged or damaged cells and the provision of specialised cells critical for tissue function. The decision to proliferate is crucial, especially for stem cells which produce daughter cells that either maintain a stem cell fate or differentiate to produce specialised cells. The rapidly-renewing intestinal epithelium replenishes its cellular content every 4-5 days. This high turnover rate is maintained primarily by Lgr5(+) intestinal stem cells in the crypt base, thought to be continually proliferative (Basak et al., 2014) as confirmed by proteomic and transcriptomic analysis (Munoz et al., 2012). There is also a quiescent stem cell-population that can re-engage with the cell-cycle to repopulate the Lgr5(+) cell population if it becomes depleted. These quiescent stem cells reside at the +4 position and constitute a subset of Lgr5(+) cells and are immature secretory lineage precursors (Buczacki et al., 2013). Lgr5(+) stem cells can divide to form transit-amplifying (TA) cells, which undergo several rounds of cell division before differentiating and losing proliferative competency (Potten and Loeffler, 1990).

How proliferative fate decisions are governed in stem cells and transit-amplifying cells is not understood. Lineage tracing studies suggest that in homeostatic intestinal tissue only 5-7 intestinal stem cells are ‘active’ out of the 12-16 Lgr5(+) cells present in the crypt base (Baker et al., 2014, Kozar et al., 2013). Interestingly, Lgr5(+) cells have a significantly longer cell-cycle than transit-amplifying cells (Schepers et al., 2011). The functional significance of the prolonged cell-cycle time of Lgr5(+) stem cells is currently unknown, but suggests active regulation of cell-cycle progression and proliferative fate commitment.

Delayed activation of the DNA replication licensing system in Lgr5(+) intestinal stem cells

Proliferative fate decisions are typically visualised by detecting markers that are present in all cell-cycle phases, and only distinguish proliferative from quiescent cells. Visualising the incorporation of labelled nucleosides such as BrdU or EdU marks cells in S-phase. The limitation of these methods is that they cannot discriminate early proliferative fate decisions made during the preceding mitosis, or in the early stages of G_1. DNA replication in S phase depends on origins having been licensed, which involves the regulated loading of minichromosome maintenance 2-7 (MCM2-7) complexes onto origins of DNA replication (reviewed in (Champeris Tsaniras et al., 2014)). During S phase, DNA-bound MCM2-7 hexamers are activated to form the catalytic core of the DNA helicase as part of the CMG (Cdc45, MCM2-7, GINS) complex (Moyer et al., 2006, Ilves et al., 2010, Makarova et al., 2012). Replication licensing is thought to occur from late mitosis throughout G_1 until passage through the restriction point (Dimitrova et al., 2002, Haland et al., 2015, Namdar and Kearsey, 2006, Symeonidou et al., 2013). Correspondingly, insufficient origin licensing directly limits the ability to progress past the restriction point causing cell cycle arrest (Alver et al., 2014, Liu et al., 2009, Shreeram et al., 2002).

When cells enter G_0, MCM2-7 proteins are transiently downregulated and degraded, primarily via E2F-mediated transcriptional control of MCM2-7, Cdc6 and Cdt1 (Leone et al., 1998, Ohtani et al., 1999, Williams et al., 1998). This prevents terminally differentiated cells from re-entering the cell cycle. In mammalian cells, artificial induction of quiescence through contact inhibition leads to gradual downregulation of Cdc6 and MCM2-7 over several days (Kingsbury et al., 2005). These features have led to the suggestion that quiescence can be defined by being an unlicensed state (Blow and Hodgson, 2002). Equally, the licensing status can define a different restriction point that signals proliferative fate

commitment at the end of mitosis and in early G_1, independently of the Rb/E2F restriction point.

The dynamics of replication licensing in the intricate cellular hierarchy of a complex, rapidly renewing adult tissue, is not understood. We therefore investigated the licensing system in the intestinal epithelium, aiming to understand dynamics of early cell-cycle commitment in stem and transit-amplifying cells and during terminal differentiation.

MATERIALS AND METHODS

Mice

All experiments were performed under UK home office guidelines. CL57BL/6 (Wild-type), *R26-rtTA Col1A1-H2B-GFP* (H2B-GFP), Lgr5-EGFP-IRES-creERT2 ($Lgr5^{GFP/+}$) and $Apc^{Min/+}$ mice were sacrificed by cervical dislocation or CO_2 asphyxiation.

Tissue preparation: Whole small intestine

Dissected pieces of adult mouse small-intestine were washed briefly in PBS and then fixed in 4% PFA for 3 hours, 4°C. Intestines were cut into 2x2 cm^2 pieces and fixed overnight in 4% PFA, 4°C. Tissue was embedded in 3% low melting temperature agarose and cut into 200 µm sections using a Vibratome (Leica). Sections were washed in PBS, permeabilised with 2% Triton-X100 for 2 hours and incubated with Blocking Buffer (1% BSA, 3% Normal Goat serum, 0.2% Triton-X100 in PBS) for 2 hours, 4°C. Tissue was incubated in Working Buffer (0.1% BSA, 0.3% Normal Goat Serum, 0.2% Triton-X100 in PBS) containing primary antibody, Mcm2 (Cell Signalling, 1:500), for 48 hours, 4°C. Sections were washed 5x with Working Buffer prior to 48 hour incubation with secondary antibodies diluted in Working Buffer:

Alexafluor™ conjugated goat anti-rabbit (1:500, Molecular Probes) plus 5 µg/ml Hoechst 33342 and Alexafluor™ conjugated Phalloidin (1:150, Molecular Probes). Sections were mounted on coverslips in Prolong Gold between 2x120 µm spacers.

Tissue preparation: Isolated Crypts

Small intestines were dissected, washed in PBS and opened longitudinally. Villi were removed by sequential scraping of the luminal surface with a coverslip. Tissue was washed in PBS, incubated in 30 mM EDTA (25 minutes, 4°C) and crypts isolated by vigorous shaking in PBS. Crypt suspensions were centrifuged (fixed rotor, 88 RCF, 4°C) and the pellet washed twice in cold PBS. Crypts were fixed in 4% PFA (30min, room temperature), permeabilized in 1% Triton-X100 (1 hour, room temperature) and blocked in Blocking Buffer (2 hours, 4°C). Crypts were incubated with primary antibodies diluted in Working Buffer: Mcm2 (Cell Signalling, 1:500), phospo-HistoneH3 (Abcam, 1:500), Ki67 (Abcam ab15580, 1:250), αGFP (Abcam, 1:500), washed 5x with Working Buffer before overnight incubation with secondary antibodies diluted in Working buffer: Alexafluor™ conjugated goat anti-mouse or anti-rabbit (1:500, Molecular Probes) or stains: Rhodamine labelled Ulex Europaeus Agglutinin I (UEA, 1:500), 5 µg/ml Hoechst 33342 or Alexafluor™ conjugated Phalloidin (1:150), at 4°C. Crypts were mounted directly on slides in Prolong Gold, overnight.

CSK extraction

Soluble proteins were extracted from the epithelial cells in isolated crypts by incubation with CSK extraction buffer (10 mM HEPES, 100 mM NaCl, 3 mM $MgCl_2$, 1 mM EGTA, 300 mM sucrose, 0.2% TritonX-100, 1 mM DTT, 2% BSA) supplemented with protease inhibitors

(PMSF, Pepstatin, Leupeptin, Cystatin, Na_3VO_4, NaF, aprotinin) for 20 minutes on ice prior to fixation. Crypts were then fixed with 4% PFA and processed further.

H2B-GFP label retention

H2B-GFP expression in transgenic *R26-rtTA Col1A1-H2B-GFP* mice was induced by replacing normal drinking water with 5% sucrose water supplemented with 2 mg/ml doxycycline. After 7 days, doxycycline water was replaced with normal drinking water. Subsequently, mice were sacrificed after 7 days.

EdU incorporation and detection

Mice were injected intraperitoneally with 100 µg EdU (Invitrogen) prepared in 200 µl sterile PBS. Mice were sacrificed 1 hour or 17 hours post induction. For organoids, 10 µM EdU was included in crypt media for 1 hour before harvesting. EdU was detected by Click-it chemistry, by incubation in EdU working buffer (1.875 µM Alexafluor 488 azide (Invitrogen), 2 mM $CuSO_4$, 10 mM Ascorbic acid), overnight at 4°C, prior to processing for immunofluorescence staining.

Organoid Culture

Isolated crypts were dissociated to single cells with TripLE express (Life Technologies) at 37°C, 5 minutes. Dissociated cells were filtered through a 40 µm cell strainer (Greiner) and suspended in growth factor reduced Matrigel (BD Biosciences). Organoids were grown in crypt media (ADF supplemented with 10 mM HEPES, 2 mM Glutamax, 1 mM N-Acetylcysteine, N2 (Gemini), B27 (Life technologies), Penicillin/Streptomycin (Sigma) supplemented with growth factors – ENR media (EGF (50 ng/ml, Invitrogen), Noggin (100

ng/ml, eBioscience) and RSpondin conditioned media produced from stably transfected L-cells (1:4). Chiron99021 (3 µM), Valproic acid (1 mM, Invitrogen) and Y27632 (10 µM, eBiosciences) were added to the culture for the first 48 hours. Organoids were passaged every 3-5 days by mechanically disrupting Matrigel and by washing and pipetting in ADF. Dissociated crypts were re-suspended in fresh Matrigel and grown in crypt media supplemented with growth factors.

For small molecule treatments, primary intestinal epithelial cells were cultured in ENR-CVY (ENR plus Chiron99021, Valproic acid and Y27632) for 3 Days, and then organoids were sub-cultured in ENR for two further days prior to the start of the experiment. Organoids were then treated with the stated small molecules for the indicated time periods. For induction of shallow-G_0, organoids were treated with Gefitinib (5 µM) coupled with removal of EGF from the crypt media. For re-activation, the media was removed and fresh growth factors added. All growth factors and inhibitors were replenished every 2 days throughout the experiment.

Flow cytometry and cell sorting

Intestinal crypts were isolated and dissociated to single cells as described above. Isolated cells were filtered through 40 µm cell strainers. Cells were fixed in 0.5% PFA (pH7.40, 15 minutes, room temperature), washed once in working buffer and permeabilized with ice-cold 70% EtOH, 10 minutes. Cells were then washed in working buffer and re-suspended with primary antibodies (Mcm2, 1:500; GFP, 1:500; Ki67, 1:200) diluted in Working buffer (overnight, 4°C). Following two washes in working buffer, cells were re-suspended in secondary antibodies goat anti-mouse or anti-rabbit (Alexafluor647, 1:500 (Molecular Probes); Alexafluor488-Ki67, 1:400 (Clone SolA15, BD Biosciences), diluted in working buffer

(1 hour, room temperature). After two washes in working buffer, cells were suspended in working buffer containing 15 µg/ml DAPI. Samples were analysed on a FACS Canto (BD Biosciences) and data analysed using FlowJo (Treestar).

For cell sorting, cells were isolated from Lgr5-GFP mice as described above by treatment with TripLE express for 15 minutes, 37ºC followed by filtration through 40 µm filters (Greiner). Cells were sorted in ADF supplemented with 1% FCS and DAPI (15 µg/ml). Sorting was performed using an Influx™ Cell sorter (BD biosciences). Cells were checked post-sort to ensure sample purity by re-examining Lgr5 expression in the sorted gates.

Microscopy and Image analysis

Samples were imaged using a Zeiss LSM 710 microscope using a 40X LD Pan-Neofluar objective lens and immersion oil with a refractive index of 1.514. Z-stacks were acquired at optimal section intervals between 0.3 and 0.8 µm.

Image processing and analysis were performed using Imaris (Bitplane). Images of individual crypts were manually cropped to ensure that an individual crypt was the only region of interest. All nuclei were detected in individual crypts using automated thresholding in Imaris, set to detect nuclei at an estimated size of 3.5 µm. Missed or incorrectly assigned nuclei were manually identified. This function produced measurement points that segmented the specific region at the corresponding co-ordinate of the measurement point. Mean intensities for different channels were calculated per spot. This equates to the intensity at the centre region of each nucleus. A reference nucleus at the crypt base was used to define the crypt base position. The Euclidean distance to this point was measured and defined as the distance to the crypt base. Multiple images were analysed using the

same workflow and the analysed files collated. For vibratome sections, a plane was manually defined running through to the muscle layer beneath the epithelium. The smallest distance to this surface was defined for segmented nuclei.

RESULTS

Mcm2 expression declines along the crypt-villus axis

Because of their abundance, strong conservation and association with the core DNA replication process, the presence of MCM2-7 proteins is frequently used to establish proliferative capacity in tissues, similar to Ki67 or PCNA (Gonzalez et al., 2005, Jurikova et al., 2016, Stoeber et al., 2001, Williams et al., 1998). Usually, terminally differentiated cells in mammalian tissues do not contain MCM2-7 (Stoeber et al., 2001, Todorov et al., 1998). To establish the overall MCM2-7 protein abundance along intestinal crypts, we first examined the expression of MCM2-7 proteins in adult murine small-intestinal epithelium using high-resolution immunofluorescence microscopy. We focused on Mcm2 as a surrogate for all the members of the MCM2-7 complex based on their similar function and localisation.

Consistent with previous reports in both murine and human intestinal epithelium, we observed that Mcm2 was highly expressed in intestinal crypts (**Figure 1A**) and declined gradually along the crypt-villus axis (**Figure 1B**), but persisted in a few cells in the villus compartment (**S1 Figure A**). MCM2-7 are highly abundant proteins and they have a relatively long (>24 hour) half-life (Musahl et al., 1998). This makes it likely that after cells differentiate, their MCM2-7 content declines at a slow rate. Mcm2 was nuclear in

194 interphase cells but cytoplasmic during mitosis (**Figure 1C**). Although the majority of
195 intestinal crypt cells expressed Mcm2, at the crypt base Mcm2(+) and Mcm2(-) cells were
196 interspersed (**Figure 1A, S1 Figure A**), consistent with previous reports (Pruitt et al., 2010).
197 This pattern is reminiscent of the alternating arrangement of Lgr5(+) stem cells and Paneth
198 cells at the crypt base (Barker et al., 2007). Lgr5(+) stem cells express Ki67 and are
199 continually proliferative whereas Paneth cells are fully differentiated and are Ki67(-) (Basak
200 et al., 2014). As expected, Mcm2 was expressed in all Lgr5(+) stem cells and there was a
201 strong correlation between Mcm2 and Lgr5 expression (**Figure 1D**). This is consistent with
202 the idea that $Lgr5^{Hi}$ stem cells are the main proliferative stem cells in the intestinal crypt.
203 Staining with Ulex Europaeus Agglutinin I (UEA), demonstrated that most of the Mcm2(-)
204 cells in the crypt base were UEA(+) Paneth cells (**Figure 1E**).

205 Normally, MCM2-7 expression is lost in terminally differentiated cells (Eward et al., 2004,
206 Stoeber et al., 2001, Williams et al., 1998, Williams et al., 2004). The loss of expression has
207 been suggested as a major contributor to the proliferation-differentiated switch *in vivo.* To
208 test this idea, we measured the Mcm2 content of young and mature secretory cells in
209 intestinal crypts and villi (**Figure 1F, G**). There was differential expression of Mcm2 in distinct
210 secretory lineages. Many mature secretory cells including Paneth, Goblet and
211 enteroendocrine cells were Mcm2(-), consistent with their differentiation status and long
212 life-span in the epithelium (van der Flier and Clevers, 2009). We detected a number of
213 UEA(+) Mcm2(+) and UEA(+) Mcm2 (-) cells in intestinal crypts (**Figure 1F**). Assuming that
214 Mcm2 expression declines slowly after differentiation, Mcm2 content could reflect the
215 maturity of a particular secretory cell. Consistently, Mcm2 expression in UEA(+) cells in

crypts was significantly higher than in villi (**Figure 1G**), supporting the idea that Mcms are gradually lost upon terminal differentiation.

Visualisation of DNA replication licensing *In vivo*

MCM2-7 exist in three states: as hexamers free in the nucleoplasm, as double hexamers bound to DNA during late mitosis, G1 and S phase, or as CMG complexes at replication forks during S phase (Evrin et al., 2009, Gambus et al., 2011, Remus et al., 2009). To distinguish between DNA-bound and soluble forms, we developed a protocol involving a brief extraction of isolated crypts with non-ionic detergent to remove soluble MCM2-7. The remaining Mcm2 should mark cells whose origins are licensed for replication. Extraction did not visibly affect intestinal crypt integrity but made them more opaque compared to unextracted tissue (**Figure 2A**). The majority of cells in unextracted crypts were Mcm2(+) (**Figure 2B**) similar to tissue sections and mirrored the ubiquitous expression of Ki67 along the crypt axis. After extraction, the majority of the Mcm2 content in cells was lost (**Figure 2B**). The labelling index of isolated crypts revealed that only 10-30% of cells were licensed (**Figure 2C**). After extraction, Mcm2(+) was not present in mitotic cells expressing phosphorylated histone H3, confirming the extraction procedure successfully removed non-DNA bound MCM2-7 proteins (**Figure 2D**).

We used flow cytometry to measure MCM2-7 content more directly and further confirm the effectiveness of the extraction procedure. Whereas the majority of isolated epithelial cells expressed Mcm2 that persisted throughout the cell-cycle, extraction revealed a distinct profile of Mcm-containing cells in crypts (**Figure 2E**) consistent with what has been reported for other cells (Friedrich et al., 2005, Moreno et al., 2016). MCM2-7s are loaded onto DNA

throughout G_1, reach a maximum level before cells enter S-phase, and are subsequently displaced from DNA during replication. Interestingly, we noticed that isolated Intestinal epithelial cells had a large range of DNA-bound Mcm2 during G_1. We propose that this represents intermediate stages of the transition between a fully quiescent G_0 state, a dormant state at the G_0/G_1 boundary or in early G_1 and a population fully committed to the cell-cycle, being fully licensed (**Figure 2E'**). Similar results were observed in cells isolated from intestinal organoids (**Figure 2F, G**)

Licensing status and cell-cycle progression along the crypt-villus axis

Cell-cycle dynamics of intestinal stem and progenitor cells are highly heterogeneous (Pruitt et al., 2010). The majority of Lgr5(+) stem cells are considered to be continually proliferative, but with a much longer cell-cycle than transit-amplifying progenitor cells, which are most commonly found in S-phase (Schepers et al., 2011). To investigate proliferative fate decisions of intestinal epithelial cells, we used our MCM2-7 extraction in crypts where S phase cells were labelled with the nucleoside analogue EdU. We then used image analysis software to correlate Mcm2 content with cell-cycle stage along the crypt-villus axis (**S1 Figure B-H**). This allowed quantification of licensing in relation to the cell-cycle and 3D spatial information.

Figure 3A shows tissue following the MCM2-7 extraction and after a short 1 hour EdU pulse to visualise S-phase. As expected, the majority of cells in the transit-amplifying compartment were labelled with EdU suggesting that most cells were in S-phase, consistent with early studies using BrdU and [^{3}H]-thymidine labelling (Chwalinski and Potten, 1987). The patterns of replication foci were consistent with the reported S-phase replication timing

programme (Rhind and Gilbert, 2013). Typically, all licensed cells had intense nuclear Mcm2 staining. Some cells completely lacked Mcm2 and EdU labelling, suggesting they could be in either G_0, very early G_1 or in G_2. Some cells were labelled with both Mcm2 and EdU. These double-labelled cells typically showed patterns of EdU labelling consistent with early to mid S phase and Mcm2 labelling of DNA compartments expected to replicate later in S phase. This relationship has been observed in tissue culture cells (Krude et al., 1996) and is consistent with the idea that DNA-bound MCM2-7 are displaced from chromosomal domains as replication is completed. Cells with late S-phase patterns of EdU labelling had little or no detectable Mcm2, consistent with the displacement of the majority of MCM2-7 by the end of S phase. Quantification of the nuclear intensities of Mcm2 and EdU in these discrete populations (**S1 Figure H**) confirmed previous results using flow cytometry (**Figure 2E**) and allowed grouping of cells into 4 cell cycle groups: Unlicensed, G_0/G_1; G_1 licensed; S-phase and Late-S/G_2 (**S1 Figure H**). We also measured nuclear volume, which increases during S phase and G_2. This showed that nuclear volume increased up to two-fold in cells classified as S-phase and Late-S/G_2 by Mcm2 and EdU staining (**Figure 3B)**. This confirms our cell-cycle assignment and also suggests that most Mcm2(-) cells are in G_0 or G_1, rather than in G_2.

The combination of concurrently labelling DNA-bound Mcm2 and EdU showed a clear correlation between cell position and cell-cycle stage (**Figure 3C, D, E**). At the base of the crypt, G_0/early-G_1 cells predominate. At increasing distances from the crypt base there is a successive rise in licensed G_1 cells, early/mid S phase cells and then late S/G_2 cells. Further up the crypt, at the end of the TA compartment, these cell cycle stages decline in reverse order, until unlicensed G_0 cells again predominate. This suggests that there is a co-ordinated

progression through the cell division cycle as cells enter, then leave, the TA compartment. This was also observed as a field effect with many neighbouring cells showing similar replication patterns (**S2 Figure A, B**).

Terminal differentiation is associated with a binary licensing decision

At the terminal boundary of the transit-amplifying compartment, the majority of cells were unlicensed and had no DNA-bound Mcm2 (**Figure 3C-E**). Similarly, there were no licensed G_1 cells beyond the TA compartment as defined by incorporation of EdU (**Figure 3F**). However, total Mcm2 expression extended significantly beyond the last cells with DNA-bound Mcm2 or incorporated EdU (**Figure 3D, F**). The distribution of total Mcm2 expression also corresponded to the zone where cells express Ki67 (**S3 Figure**). Although Mcm2 and Ki67 expression persists beyond the TA compartment, licensing does not occur in this area. This suggests that differentiation is not governed by a gradual reduction in total MCM2-7 levels, but is a binary decision and licensing is abolished immediately after the final mitosis preceding differentiation. To further examine this, we marked the terminally differentiated zone by a 1 hour EdU pulse, followed by a 16 hour chase (**Figure 3G, H**). After 16 hours, the majority of the distal end of the TA compartment became labelled with EdU. All labelled nuclei in this area were significantly smaller than EdU(+) cells at the proximal end of the TA compartment (data not shown), suggestive of their differentiation status. Importantly the EdU(+) differentiated cells at the distal end of the TA compartment lacked DNA-bound Mcm2, supportive of the model where licensing is inhibited immediately at terminal differentiation.

The majority of Intestinal stem cells reside in unlicensed shallow-G_0' state

The majority of cells in the crypt base expressed Mcm2, consistent with the finding that all Lgr5(+) cells express Mcm2 but mature secretory cells, such as Paneth cells, do not (**Figure 1D, E**). Surprisingly, extraction revealed that only 7-15% of cells were licensed in the crypt base (**Figure 3C, D**), with most cells in an unlicensed state despite expressing Mcm2. The abundance of licensed cells peaked 40-60 µm away from the crypt base, corresponding to just above the +4/+5 cell position (**Figure 3D, E**).

It is not possible to identify Lgr5 in these experiments, as it is extracted along with unbound Mcm2. We therefore identified Paneth cells by UEA staining and considered all UEA(-) cells in the crypt base to be intestinal stem cells (**Figure 4A**). >50% of the UEA(-) stem cells were in an unlicensed state and were not incorporating EdU (**Figure 4B**). Approximately 30-40% of all UEA(-) cells in the stem cell compartment were in an active phase of the cell cycle, (**Figure 4B**) corresponding to 5-6 stem cells out of the total 14 present (Snippert et al., 2010). This number is similar to the small number of proposed 'working' stem cells in the crypt base (Baker et al., 2014, Kozar et al., 2013). Unlicensed cells not incorporating EdU (i.e. unlabelled in this experiment) could theoretically be in either G_0 or in G_2. To distinguish between these possibilities we first isolated crypt cells from Lgr5-GFP mice and measured both GFP and DNA content. Both Lgr5(+) and Lgr5(-) cell populations had a similar cell-cycle profile with the majority of cells having 2N DNA content (**S2 Figure C**). We also examined the nuclear volume of cells at different positions along the crypt axis, after staining for EdU incorporation and DNA-bound Mcm2. The majority of unlicensed cells had a similar nuclear volume to fully licensed cells in G_1 and not cells in Late-S/G_2 phase (**S2 Figure D**). Together,

these results suggest that, although they express abundant Mcm2, the majority of intestinal stem cells reside in an unlicensed state.

To confirm this conclusion, we flow sorted Lgr5-GFP(+) cells, extracted unbound MCM2-7 and stained them for Mcm2 and Ki67. Consistent with our previous results, most of the Lgr5(+) cells with a 2N DNA content had low levels of DNA-bound Mcm2, and were in an unlicensed state (**Figure 4Ci, ii**). Importantly, both the licensed and unlicensed cells were Ki67(+) indicating that they had not withdrawn from the cell-cycle long-term (**Figure 4Cii**).

This state – 2N DNA content with low levels of DNA-bound Mcm2 - could be explained by two, slightly different, scenarios. One possibility is that MCM2-7 are loaded on to DNA very slowly in Lgr5(+) cells, thereby extending G_1 length (Schepers et al., 2011) (Dalton, 2015). In this case, the presence of unlicensed cells simply reflects the increased time required to fully license origins, and different levels of Mcm2 loading should be equally distributed between G_1 cells. Alternatively, most Lgr5(+) cells are not in G_1 and do not load MCM2-7 until an active decision is made to enter the cell cycle and activate the licensing system, at which time MCM2-7 proteins are rapidly loaded. In this case, there should be a discrete peak of unlicensed cells with a G_1 DNA content representing cells that have withdrawn from the cell cycle, and a lower frequency of G_1 cells that have loaded different amounts of MCM2-7. To distinguish between these two possibilities, we examined the frequency distribution of DNA-bound Mcm2 in Lgr5(+) cells with a 2N DNA content (**Figure 4Ciii**). The distribution of DNA-bound Mcm2 cells was most similar to the predicted distribution in the latter model and showed a discrete peak of unlicensed cells (**Figure 4C**). Since most of these unlicensed Lgr5(+) cells express abundant Mcm2 (**Figure 1D**), they are in a state that is distinct from that of previously described G_0 cells, which typically do not express licensing

proteins at all. We term this new intermediate state – where cells express abundant MCM2-7 proteins that are not bound to DNA – as 'shallow-G_0'. Because they do not need to synthesize more MCM2-7 proteins to enter the cell cycle, they are likely to be in a transient state of quiescence.

It has previously been reported that embryonic stem cells license more replication origins than neural stem/progenitor cells differentiated from them (Ge et al., 2015). To determine if stem and non-stem cells in intestinal crypts behave similarly, we compared the amount of DNA-bound Mcm2 in G_1/G_0 and early S phase Lgr5(+) cells with that in Lgr5(-) cells (Moreno et al., 2016). Although the majority of Lgr5(+) cells were unlicensed, when they entered S phase they had approximately twice as much DNA-bound Mcm2 compared to Lgr5(-) cells (**Figure 4D**). This is consistent with the idea that adult intestinal stem cells license more origins than TA cells. This may represent a mechanism to protect genomic integrity.

Intestinal label retaining cells are in a deep G_0 state

Although the intestinal crypt base primarily consists of Lgr5(+) stem cells there is also a reserved pool of quiescent stem cells, often referred to as '+4 label retaining cells' (LRCs) reflecting their position in the crypt base and their ability to retain nascent DNA labels (Potten et al., 2002). These cells are a rare subset of Lgr5(+) cells which are also secretory precursors (Buczacki et al., 2013). To further define the licensing status of these label-retaining intestinal stem cells, we identified UEA(-) LRCs by expressing H2B-GFP (which is incorporated into the chromatin of dividing cells) for 7 days and then chasing for a further 7 days (**S4 Figure**) (Buczacki et al., 2013, Roth et al., 2012). Labelled cells that did not divide during the 7-day chase period contain high levels of H2B-GFP, and cells that divided multiple

times only have low levels. Strikingly, unlike the majority of the Lgr5(+) cells, quiescent LRCs with high GFP-H2B did not express Mcm2 (**Figure 4E**). Consistently, only non-LRC daughter cells with low levels of H2B-GFP had DNA-bound Mcm2 (**Figure 4F, G**). This shows that, as expected, the LRC stem cells are in deep G_0, unable to license because they do not express MCM2-7. In contrast, the 'active' intestinal stem cells reside in a state of shallow G_0, expressing MCM2-7, but remain unlicensed.

Stemness is associated with the unlicensed state

We wished to understand how intestinal stem cells were maintained in an unlicensed state and whether stemness was directly associated with the unlicensed shallow-G_0 state. To investigate this relationship we designed a proof-of-concept assay using intestinal organoids. This allowed a preliminary assessment of licensing dynamics during entry and exit into quiescence. In contrast to intestinal crypts *in vivo*, intestinal organoids contained considerably more cells with DNA-bound Mcm2 in their crypt-like branches (**Figure 5A**). Cytometry-based quantification of cells with a 2N DNA content suggested that there were approximately twice as many fully licensed cells in organoids than in intestinal crypts (**Figure 5Bi, ii**). This suggests that organoids may represent intestinal epithelium in an accelerated state of self-renewal and do not fully recapitulate cell-cycle dynamics of intestinal epithelial cells *in vivo*.

To measure licensing dynamics in organoids during entry and exit into quiescence, we directly compared licensing states with the presence of Ki67. Most cells in organoids express Ki67 and it increased during cell-cycle progression (**Figure 5Ci**). The DNA-bound Mcm2 profile was similar to that in isolated crypts (compare **Figure 5Cii** and Figure 2E). Correlating

Ki67 and DNA-bound Mcm2 produced a distinctive profile that is similar for isolated cells from organoids and intestinal crypts. This profile reveals a population of cells that appear to be losing Ki67 (dashed arrow in **Figure 5 Ciii and iv**) and which might represent cells losing proliferative capacity and transitioning towards differentiation (**Figure 5C, S5 Figure A**). This loss of proliferative capacity may begin in cells that express Ki67 but are unlicensed, i.e. cells in shallow G_0. It also suggests that different stages of quiescence exist that are reflected by a spectrum of Ki67 and Mcm levels. To test this idea, we induced quiescence by inhibiting the EGF receptor (EGFR), which reduces MAP kinase activity and blocks DNA replication and cell division (Lynch et al., 2004). Strikingly, inhibition of EGFR for 24 hours induced arrest in shallow-G_0, and caused the majority of cells to be unlicensed with a 2N DNA content, while expressing Mcm2 and Ki67 (**Figure 5Dii**). Prolonged EGFR inhibition caused a transition into an intermediate state between shallow-G_0 and deep G_0, with reduced Ki67 expression but with total Mcm2 levels maintained (**Figure 5Diii**). These shallow-G_0 states were reversible by removal of EGFRi and re-addition of fresh growth factors (**Figure 5Div**).

We also used this assay to investigate how these shallow-G_0 states and stemness might be related. Inhibiting EGFR also increases Lgr5 expression (Basak et al., 2017), suggesting that prolonged quiescence can be associated with 'stemness'. The observed increase in shallow G_0 cells after 24 hours EGFRi treatment is thus consistent with the idea that stem cells spend time in shallow G_0. To test this idea more directly, we also used an alternative approach. Treatment of organoids with Chir99201 (a GS3K inhibitor) and Valproic acid (a Notch activator/histone deacetylase inhibitor) resulted in Lgr5 expression throughout the organoid epithelium (**S5 Figure B**) (Yin et al., 2014). This treatment also caused the appearance of a population of cells with low levels of Ki67 and intermediate levels of DNA-bound Mcm2

(**Figure 5E**) similar to the intermediate shallow G_0 state caused by EGFRi. Surprisingly, we observed cells with low levels of Ki67 and intermediate levels of DNA-bound Mcm2, suggesting that re-licensing of these cells occurs before they express high levels of Ki67. Making measurements at intermediate times of CV treatment or after CV removal, confirmed the existence of the intermediate and shallow G_0 states and also the ability to re-license before Ki67 re-expression (**Figure 5F**). Combining EGFRi and CV treatment, also suggested that cells can reactivated licensing from the intermediate G_0 state directly (**Figure 5G**).

Treatment with Valproic acid alone, but not Chir99021, partially recapitulated this effect, suggesting that active Notch signalling is involved (**S5 Figure C**). Inhibiting Notch signalling with DAPT treatment, which induces terminal secretory cell differentiation (van Es et al., 2005), caused an induction of deep-G_0, with reduced Ki67 and a loss of Mcm2 proteins (**S5 Figure D**). Together, this suggests that Notch signalling can affect the transition between deep and shallow-G_0 states.

Discussion

The cell-cycle of intestinal stem and transit-amplifying cells is poorly understood. By comparing the total and DNA-bound Mcm2 in intact intestinal crypts we provide new insights into how licensing and cell-cycle commitment are coupled in this tissue. We provide evidence that after their final mitosis, transit amplifying cells do not license their replication origins and so immediately exit the cell cycle. We show that normally the majority of Lgr5(+) stem cells reside in an unlicensed state, despite expressing Mcm2 and Ki67. In this state of shallow-G_0, stem cells might be poised to easily re-enter the cell division cycle.

Lgr5(+) stem cells have a cell-cycle length greater than transit-amplifying cells (Schepers et al., 2011). The biological relevance of this is currently unknown. The data presented here suggest a delay in origin licensing is responsible for the prolonged cell-cycle of Lgr5(+) cells. Although ~80% of Lgr5(+) cells are thought to be continually proliferative and express high levels of both Ki67 (Basak et al., 2014) and Mcm2, we found that most Lgr5(+) cells reside in an unlicensed state, with 2N DNA content and Mcm2 not bound to DNA. Since the licensed state defines proliferative fate commitment, we suggest that these cells are in a prolonged state of shallow quiescence, which we term shallow G_0, expressing proliferative makers such as Ki67 and Mcm2 without committing to proliferation since Mcm2 is not bound to DNA (**Figure 6**). The number of Lgr5(+) cells with DNA bound-Mcm2 was similar to the number of proposed 'active' stem cells determined in lineage tracing experiments (Baker et al., 2014, Kozar et al., 2013).

Prolonged arrest may eventually result in degradation of MCM2-7 proteins and lead to induction of a state of deep quiescence. Consistent with this idea, we observed that LRCs, thought to provide a reserve of quiescent stem cells, did not express Mcm2. The lack of Mcm2 expression may reflect that a significant period of time has passed since these cells divided. The delay in activating the licensing system may create a prolonged time-window for Lgr5(+) cells to receive and interpret environmental cues before deciding to commit to duplication, offering a means to control their number. It is likely that the majority of Lgr5(+) cells eventually re-enter the cell cycle, given their continual expression of proliferation markers (Basak et al., 2014). The identity and decisions of Lgr5(+) cells are likely governed by stochastic choices and the ability to enter a shallow G_0 stage offers unique flexibility for stem cells to make these choices. Consistent with this idea, modulation of the stem cell

niche by Chir99021 and Valproic acid induces stemness throughout the crypt-villus axis (Yin et al., 2014) and also significantly enriches a unique population of unlicensed cells with unique cell-cycle dynamics. The increase in Lgr5(+) cells in response to Valproic acid and Chir99021 suggests a corresponding increase in the number of Lgr5(+) reserve stem cells, which are in deep G_0 (Buczacki et al., 2013). We propose that the reactivation of these cells by injury for instance, could proceed via the intermediate G_0 state we describe. Initially, these cells must re-express Mcm proteins and then can directly commit to the cell-cycle from the intermediat-G_0 state (**S5 Figure E**). Together, this demonstrates the unique cell-cycle characteristics of intestinal stem cells, which can be functionally defined by the licensed state.

Growing evidence suggests that intestinal stem cell fate is not governed by asymmetric segregation of fate determinants (Lopez-Garcia et al., 2010, Snippert et al., 2010, Steinhauser et al., 2012). Components of the stem cell niche, such as the combination of Wnt and Notch signalling can affect stem cell fate decisions and also reduce the cycle rate of intestinal stem cells (Hirata et al., 2013). This is consistent with the idea that as well as decreasing proliferation rate, increased G_0/G_1 length might underpin cell fate choices. Indeed, G_1 elongation of mouse and human embryonic stem cells can drive differentiation (Calder et al., 2013, Coronado et al., 2013). Similarly, long G_1 phases are associated with the production of fate-restricted progenitors during neurogenesis (Arai et al., 2011). This has been suggested to be facilitated by an extended time window in the cell-cycle to allow niche factors and/or fate determinants to (Calegari and Huttner, 2003). In the case of intestinal stem cells, holding cells in shallow G_0 may allow an extended time for stem cell fate factors to act and maintain stem cell fate.

Like embryonic stem cells (Ge et al., 2015), intestinal stem cells appear to have licensed more origins than non-stem cells when they enter S phase. Intestinal stem cells may therefore more readily engage the licensing checkpoint that ensures that all origins are licensed before cells enter S phase (Alver et al., 2014, Liu et al., 2009, Shreeram et al., 2002). This additional demand for licensed origins in stem cells may explain why crypts hypomorphic for Mcm2 have a stem-cell deficiency (Pruitt et al., 2007).

Terminal differentiation in the intestinal epithelium is associated with disengagement from the proliferative niche and involves the gradual dilution of niche factors, which causes cells to exit the cell-cycle (Farin et al., 2016, Mariadason et al., 2005). Consistent with previous reports, we observed that Mcm2 expression gradually declined along the crypt-villus axis (**Figure 1**) (Stoeber et al., 2001). We also found that there is an abrupt loss of DNA-bound Mcm2 as cells exit the transit amplifying zone and undergo terminal differentiation. This suggests that the proliferation-differentiation switch is a binary decision made in the last cell cycle in the mid-upper transit-amplifying compartment.

It is unclear why licensing is rapidly inhibited at the top of the transit amplifying zone or in most of the Lgr5(+) stem cells. The simplest explanation is that licensing factors such as Cdt1 or Cdc6 are not readily available in new-born stem cells, and their synthesis has to be directed by an upstream signal for fate commitment. This occurs after prolonged quiescence which is accompanied by passive downregulation of such licensing factors (Coller, 2007). In contrast, in continually dividing cells their levels are maintained. Consistently, licensing factors such as Cdc6, along with many cyclin-CDK complexes, are down regulated beyond the end of the TA zone (Frey et al., 2000) (Smartt et al., 2007).

In summary, we demonstrate that the dynamics of the DNA replication licensing system provides a new way of measuring the proliferative fate of intestinal stem cells. We suggest a model for 'working' intestinal stem cells that reside in a state of shallow quiescence until a proliferative fate decision is made. Consistent exit from the cell-cycle in label retaining '+4' cells leads to loss of proliferative capacity and loss of Mcm2 expression causing cells to enter a deeply quiescent state (**Figure 6**). We suggest that the shallow-G_0 state serves stem cells in controlling their numbers by regulating the cell-cycle.

Author contributions

T.D.C, J.J.B and I.N conceived and designed the study; T.D.C collected the data and performed the analysis; I.P.N assisted with animal experiments; T.D.C wrote the manuscript with assistance from I.N and J.J.B.

Conflicts of Interest

The authors report no conflicts of interest.

Acknowledgements

We would like to thank members of the Näthke and Blow laboratories for general assistance and helpful discussions. We thank Dr Paul Appleton, Dr Graeme Ball and the Dundee Imaging and Tissue Imaging Facility for support with microscopy and image analysis. The imaging facility is funded by the Welcome Trust Technology Platform award (097945/B/11/Z) and Welcome Trust award (101468/Z/13/Z). We thank Dr Rosemary Clarke and the Dundee Flow Cytometry Facility for support with flow cytometry, cell sorting and analysis. This work was supported by a programme grant from Cancer Research UK to I.N

(C430/A11243) and to J.J.B (C303/A14301), Wellcome Trust grant WT096598MA and an MRC studentship award to T.D.C.

REFERENCES

ALVER, R. C., CHADHA, G. S. & BLOW, J. J. 2014. The contribution of dormant origins to genome stability: from cell biology to human genetics. *DNA repair,* 19**,** 182-9.

ARAI, Y., PULVERS, J. N., HAFFNER, C., SCHILLING, B., NUSSLEIN, I., CALEGARI, F. & HUTTNER, W. B. 2011. Neural stem and progenitor cells shorten S-phase on commitment to neuron production. *Nature communications,* 2**,** 154.

BAKER, A. M., CERESER, B., MELTON, S., FLETCHER, A. G., RODRIGUEZ-JUSTO, M., TADROUS, P. J., HUMPHRIES, A., ELIA, G., MCDONALD, S. A., WRIGHT, N. A., SIMONS, B. D., JANSEN, M. & GRAHAM, T. A. 2014. Quantification of crypt and stem cell evolution in the normal and neoplastic human colon. *Cell reports,* 8**,** 940-7.

BARKER, N., VAN ES, J. H., KUIPERS, J., KUJALA, P., VAN DEN BORN, M., COZIJNSEN, M., HAEGEBARTH, A., KORVING, J., BEGTHEL, H., PETERS, P. J. & CLEVERS, H. 2007. Identification of stem cells in small intestine and colon by marker gene Lgr5. *Nature,* 449**,** 1003-7.

BASAK, O., BEUMER, J., WIEBRANDS, K., SENO, H., VAN OUDENAARDEN, A. & CLEVERS, H. 2017. Induced Quiescence of Lgr5+ Stem Cells in Intestinal Organoids Enables Differentiation of Hormone-Producing Enteroendocrine Cells. *Cell stem cell,* 20**,** 177-190 e4.

BASAK, O., VAN DE BORN, M., KORVING, J., BEUMER, J., VAN DER ELST, S., VAN ES, J. H. & CLEVERS, H. 2014. Mapping early fate determination in Lgr5+ crypt stem cells using a novel Ki67-RFP allele. *The EMBO journal,* 33**,** 2057-68.

BLOW, J. J. & HODGSON, B. 2002. Replication licensing--defining the proliferative state? *Trends in cell biology,* 12**,** 72-8.

BUCZACKI, S. J., ZECCHINI, H. I., NICHOLSON, A. M., RUSSELL, R., VERMEULEN, L., KEMP, R. & WINTON, D. J. 2013. Intestinal label-retaining cells are secretory precursors expressing Lgr5. *Nature,* 495**,** 65-9.

CALDER, A., ROTH-ALBIN, I., BHATIA, S., PILQUIL, C., LEE, J. H., BHATIA, M., LEVADOUX-MARTIN, M., MCNICOL, J., RUSSELL, J., COLLINS, T. & DRAPER, J. S. 2013. Lengthened G1 phase indicates differentiation status in human embryonic stem cells. *Stem cells and development,* 22**,** 279-95.

CALEGARI, F. & HUTTNER, W. B. 2003. An inhibition of cyclin-dependent kinases that lengthens, but does not arrest, neuroepithelial cell cycle induces premature neurogenesis. *Journal of cell science,* 116**,** 4947-55.

CHAMPERIS TSANIRAS, S., KANELLAKIS, N., SYMEONIDOU, I. E., NIKOLOPOULOU, P., LYGEROU, Z. & TARAVIRAS, S. 2014. Licensing of DNA replication, cancer, pluripotency and differentiation: an interlinked world? *Seminars in cell & developmental biology,* 30**,** 174-80.

CHWALINSKI, S. & POTTEN, C. S. 1987. Influence of irradiation or thymidine (TdR) on the pattern of 3H-TdR incorporation at each cell position in the crypts of the small intestine of the mouse. *International journal of radiation biology and related studies in physics, chemistry, and medicine,* 51**,** 243-54.

COLLER, H. A. 2007. What's taking so long? S-phase entry from quiescence versus proliferation. *Nature reviews. Molecular cell biology,* 8**,** 667-70.

CORONADO, D., GODET, M., BOURILLOT, P. Y., TAPPONNIER, Y., BERNAT, A., PETIT, M., AFANASSIEFF, M., MARKOSSIAN, S., MALASHICHEVA, A., IACONE, R., ANASTASSIADIS, K. & SAVATIER, P. 2013. A short G1 phase is an intrinsic determinant of naive embryonic stem cell pluripotency. *Stem cell research,* 10**,** 118-31.

DALTON, S. 2015. Linking the Cell Cycle to Cell Fate Decisions. *Trends in cell biology,* 25**,** 592-600.

DIMITROVA, D. S., PROKHOROVA, T. A., BLOW, J. J., TODOROV, I. T. & GILBERT, D. M. 2002. Mammalian nuclei become licensed for DNA replication during late telophase. *Journal of cell science,* 115**,** 51-9.

EVRIN, C., CLARKE, P., ZECH, J., LURZ, R., SUN, J., UHLE, S., LI, H., STILLMAN, B. & SPECK, C. 2009. A double-hexameric MCM2-7 complex is loaded onto origin DNA during licensing of eukaryotic DNA replication. *Proceedings of the National Academy of Sciences of the United States of America,* 106**,** 20240-5.

EWARD, K. L., OBERMANN, E. C., SHREERAM, S., LODDO, M., FANSHAWE, T., WILLIAMS, C., JUNG, H. I., PREVOST, A. T., BLOW, J. J., STOEBER, K. & WILLIAMS, G. H. 2004. DNA replication licensing in somatic and germ cells. *Journal of cell science,* 117**,** 5875-86.

FARIN, H. F., JORDENS, I., MOSA, M. H., BASAK, O., KORVING, J., TAURIELLO, D. V., DE PUNDER, K., ANGERS, S., PETERS, P. J., MAURICE, M. M. & CLEVERS, H. 2016. Visualization of a short-range Wnt gradient in the intestinal stem-cell niche. *Nature,* 530**,** 340-3.

FREY, M. R., CLARK, J. A., LEONTIEVA, O., URONIS, J. M., BLACK, A. R. & BLACK, J. D. 2000. Protein kinase C signaling mediates a program of cell cycle withdrawal in the intestinal epithelium. *The Journal of cell biology,* 151**,** 763-78.

FRIEDRICH, T. D., BEDNER, E., DARZYNKIEWICZ, Z. & LEHMAN, J. M. 2005. Distinct patterns of MCM protein binding in nuclei of S phase and rereplicating SV40-infected monkey kidney cells. *Cytometry. Part A : the journal of the International Society for Analytical Cytology,* 68**,** 10-8.

GAMBUS, A., KHOUDOLI, G. A., JONES, R. C. & BLOW, J. J. 2011. MCM2-7 form double hexamers at licensed origins in Xenopus egg extract. *The Journal of biological chemistry,* 286**,** 11855-64.

GE, X. Q., HAN, J., CHENG, E. C., YAMAGUCHI, S., SHIMA, N., THOMAS, J. L. & LIN, H. 2015. Embryonic Stem Cells License a High Level of Dormant Origins to Protect the Genome against Replication Stress. *Stem cell reports,* 5**,** 185-94.

GONZALEZ, M. A., TACHIBANA, K. E., LASKEY, R. A. & COLEMAN, N. 2005. Control of DNA replication and its potential clinical exploitation. *Nature reviews. Cancer,* 5**,** 135-41.

HALAND, T. W., BOYE, E., STOKKE, T., GRALLERT, B. & SYLJUASEN, R. G. 2015. Simultaneous measurement of passage through the restriction point and MCM loading in single cells. *Nucleic acids research,* 43**,** e150.

HIRATA, A., UTIKAL, J., YAMASHITA, S., AOKI, H., WATANABE, A., YAMAMOTO, T., OKANO, H., BARDEESY, N., KUNISADA, T., USHIJIMA, T., HARA, A., JAENISCH, R.,

HOCHEDLINGER, K. & YAMADA, Y. 2013. Dose-dependent roles for canonical Wnt signalling in de novo crypt formation and cell cycle properties of the colonic epithelium. *Development,* 140**,** 66-75.

ILVES, I., PETOJEVIC, T., PESAVENTO, J. J. & BOTCHAN, M. R. 2010. Activation of the MCM2-7 helicase by association with Cdc45 and GINS proteins. *Molecular cell,* 37**,** 247-58.

JURIKOVA, M., DANIHEL, L., POLAK, S. & VARGA, I. 2016. Ki67, PCNA, and MCM proteins: Markers of proliferation in the diagnosis of breast cancer. *Acta histochemica,* 118**,** 544-52.

KINGSBURY, S. R., LODDO, M., FANSHAWE, T., OBERMANN, E. C., PREVOST, A. T., STOEBER, K. & WILLIAMS, G. H. 2005. Repression of DNA replication licensing in quiescence is independent of geminin and may define the cell cycle state of progenitor cells. *Experimental cell research,* 309**,** 56-67.

KOZAR, S., MORRISSEY, E., NICHOLSON, A. M., VAN DER HEIJDEN, M., ZECCHINI, H. I., KEMP, R., TAVARE, S., VERMEULEN, L. & WINTON, D. J. 2013. Continuous clonal labeling reveals small numbers of functional stem cells in intestinal crypts and adenomas. *Cell stem cell,* 13**,** 626-33.

KRUDE, T., MUSAHL, C., LASKEY, R. A. & KNIPPERS, R. 1996. Human replication proteins hCdc21, hCdc46 and P1Mcm3 bind chromatin uniformly before S-phase and are displaced locally during DNA replication. *Journal of cell science,* 109 (Pt 2)**,** 309-18.

LEONE, G., DEGREGORI, J., YAN, Z., JAKOI, L., ISHIDA, S., WILLIAMS, R. S. & NEVINS, J. R. 1998. E2F3 activity is regulated during the cell cycle and is required for the induction of S phase. *Genes & development,* 12**,** 2120-30.

LIU, P., SLATER, D. M., LENBURG, M., NEVIS, K., COOK, J. G. & VAZIRI, C. 2009. Replication licensing promotes cyclin D1 expression and G1 progression in untransformed human cells. *Cell cycle,* 8**,** 125-36.

LOPEZ-GARCIA, C., KLEIN, A. M., SIMONS, B. D. & WINTON, D. J. 2010. Intestinal stem cell replacement follows a pattern of neutral drift. *Science,* 330**,** 822-5.

LYNCH, T. J., BELL, D. W., SORDELLA, R., GURUBHAGAVATULA, S., OKIMOTO, R. A., BRANNIGAN, B. W., HARRIS, P. L., HASERLAT, S. M., SUPKO, J. G., HALUSKA, F. G., LOUIS, D. N., CHRISTIANI, D. C., SETTLEMAN, J. & HABER, D. A. 2004. Activating mutations in the epidermal growth factor receptor underlying responsiveness of non-small-cell lung cancer to gefitinib. *The New England journal of medicine,* 350**,** 2129-39.

MAKAROVA, K. S., KOONIN, E. V. & KELMAN, Z. 2012. The CMG (CDC45/RecJ, MCM, GINS) complex is a conserved component of the DNA replication system in all archaea and eukaryotes. *Biology direct,* 7**,** 7.

MARIADASON, J. M., NICHOLAS, C., L'ITALIEN, K. E., ZHUANG, M., SMARTT, H. J., HEERDT, B. G., YANG, W., CORNER, G. A., WILSON, A. J., KLAMPFER, L., ARANGO, D. & AUGENLICHT, L. H. 2005. Gene expression profiling of intestinal epithelial cell maturation along the crypt-villus axis. *Gastroenterology,* 128**,** 1081-8.

MORENO, A., CARRINGTON, J. T., ALBERGANTE, L., AL MAMUN, M., HAAGENSEN, E. J., KOMSELI, E. S., GORGOULIS, V. G., NEWMAN, T. J. & BLOW, J. J. 2016. Unreplicated DNA remaining from unperturbed S phases passes through mitosis for resolution in daughter cells. *Proceedings of the National Academy of Sciences of the United States of America,* 113**,** E5757-64.

MOYER, S. E., LEWIS, P. W. & BOTCHAN, M. R. 2006. Isolation of the Cdc45/Mcm2-7/GINS (CMG) complex, a candidate for the eukaryotic DNA replication fork helicase. *Proceedings of the National Academy of Sciences of the United States of America,* 103**,** 10236-41.

MUNOZ, J., STANGE, D. E., SCHEPERS, A. G., VAN DE WETERING, M., KOO, B. K., ITZKOVITZ, S., VOLCKMANN, R., KUNG, K. S., KOSTER, J., RADULESCU, S., MYANT, K., VERSTEEG, R., SANSOM, O. J., VAN ES, J. H., BARKER, N., VAN OUDENAARDEN, A., MOHAMMED, S., HECK, A. J. & CLEVERS, H. 2012. The Lgr5 intestinal stem cell signature: robust expression of proposed quiescent '+4' cell markers. *The EMBO journal,* 31**,** 3079-91.

MUSAHL, C., HOLTHOFF, H. P., LESCH, R. & KNIPPERS, R. 1998. Stability of the replicative Mcm3 protein in proliferating and differentiating human cells. *Experimental cell research,* 241**,** 260-4.

NAMDAR, M. & KEARSEY, S. E. 2006. Analysis of Mcm2-7 chromatin binding during anaphase and in the transition to quiescence in fission yeast. *Experimental cell research,* 312**,** 3360-9.

OHTANI, K., IWANAGA, R., NAKAMURA, M., IKEDA, M., YABUTA, N., TSURUGA, H. & NOJIMA, H. 1999. Cell growth-regulated expression of mammalian MCM5 and MCM6 genes mediated by the transcription factor E2F. *Oncogene,* 18**,** 2299-309.

POTTEN, C. S. & LOEFFLER, M. 1990. Stem cells: attributes, cycles, spirals, pitfalls and uncertainties. Lessons for and from the crypt. *Development,* 110**,** 1001-20.

POTTEN, C. S., OWEN, G. & BOOTH, D. 2002. Intestinal stem cells protect their genome by selective segregation of template DNA strands. *Journal of cell science,* 115**,** 2381-8.

PRUITT, S. C., BAILEY, K. J. & FREELAND, A. 2007. Reduced Mcm2 expression results in severe stem/progenitor cell deficiency and cancer. *Stem cells,* 25**,** 3121-32.

PRUITT, S. C., FREELAND, A. & KUDLA, A. 2010. Cell cycle heterogeneity in the small intestinal crypt and maintenance of genome integrity. *Stem cells,* 28**,** 1250-9.

REMUS, D., BEURON, F., TOLUN, G., GRIFFITH, J. D., MORRIS, E. P. & DIFFLEY, J. F. 2009. Concerted loading of Mcm2-7 double hexamers around DNA during DNA replication origin licensing. *Cell,* 139**,** 719-30.

RHIND, N. & GILBERT, D. M. 2013. DNA replication timing. *Cold Spring Harbor perspectives in biology,* 5**,** a010132.

ROTH, S., FRANKEN, P., SACCHETTI, A., KREMER, A., ANDERSON, K., SANSOM, O. & FODDE, R. 2012. Paneth cells in intestinal homeostasis and tissue injury. *PloS one,* 7**,** e38965.

SCHEPERS, A. G., VRIES, R., VAN DEN BORN, M., VAN DE WETERING, M. & CLEVERS, H. 2011. Lgr5 intestinal stem cells have high telomerase activity and randomly segregate their chromosomes. *The EMBO journal,* 30**,** 1104-9.

SHREERAM, S., SPARKS, A., LANE, D. P. & BLOW, J. J. 2002. Cell type-specific responses of human cells to inhibition of replication licensing. *Oncogene,* 21**,** 6624-32.

SMARTT, H. J., GUILMEAU, S., NASSER, S. V., NICHOLAS, C., BANCROFT, L., SIMPSON, S. A., YEH, N., YANG, W., MARIADASON, J. M., KOFF, A. & AUGENLICHT, L. H. 2007. p27kip1 Regulates cdk2 activity in the proliferating zone of the mouse intestinal epithelium: potential role in neoplasia. *Gastroenterology,* 133**,** 232-43.

SNIPPERT, H. J., VAN DER FLIER, L. G., SATO, T., VAN ES, J. H., VAN DEN BORN, M., KROON-VEENBOER, C., BARKER, N., KLEIN, A. M., VAN RHEENEN, J., SIMONS, B. D. & CLEVERS, H. 2010. Intestinal crypt homeostasis results from neutral competition between symmetrically dividing Lgr5 stem cells. *Cell,* 143**,** 134-44.

704 STEINHAUSER, M. L., BAILEY, A. P., SENYO, S. E., GUILLERMIER, C., PERLSTEIN, T. S., GOULD,
705 A. P., LEE, R. T. & LECHENE, C. P. 2012. Multi-isotope imaging mass spectrometry
706 quantifies stem cell division and metabolism. *Nature,* 481**,** 516-9.
707 STOEBER, K., TLSTY, T. D., HAPPERFIELD, L., THOMAS, G. A., ROMANOV, S., BOBROW, L.,
708 WILLIAMS, E. D. & WILLIAMS, G. H. 2001. DNA replication licensing and human cell
709 proliferation. *Journal of cell science,* 114**,** 2027-41.
710 SYMEONIDOU, I. E., KOTSANTIS, P., ROUKOS, V., RAPSOMANIKI, M. A., GRECCO, H. E.,
711 BASTIAENS, P., TARAVIRAS, S. & LYGEROU, Z. 2013. Multi-step loading of human
712 minichromosome maintenance proteins in live human cells. *The Journal of biological*
713 *chemistry,* 288**,** 35852-67.
714 TODOROV, I. T., WERNESS, B. A., WANG, H. Q., BUDDHARAJU, L. N., TODOROVA, P. D.,
715 SLOCUM, H. K., BROOKS, J. S. & HUBERMAN, J. A. 1998. HsMCM2/BM28: a novel
716 proliferation marker for human tumors and normal tissues. *Laboratory investigation;*
717 *a journal of technical methods and pathology,* 78**,** 73-8.
718 VAN DER FLIER, L. G. & CLEVERS, H. 2009. Stem cells, self-renewal, and differentiation in the
719 intestinal epithelium. *Annual review of physiology,* 71**,** 241-60.
720 VAN ES, J. H., VAN GIJN, M. E., RICCIO, O., VAN DEN BORN, M., VOOIJS, M., BEGTHEL, H.,
721 COZIJNSEN, M., ROBINE, S., WINTON, D. J., RADTKE, F. & CLEVERS, H. 2005.
722 Notch/gamma-secretase inhibition turns proliferative cells in intestinal crypts and
723 adenomas into goblet cells. *Nature,* 435**,** 959-63.
724 WILLIAMS, G. H., ROMANOWSKI, P., MORRIS, L., MADINE, M., MILLS, A. D., STOEBER, K.,
725 MARR, J., LASKEY, R. A. & COLEMAN, N. 1998. Improved cervical smear assessment
726 using antibodies against proteins that regulate DNA replication. *Proceedings of the*
727 *National Academy of Sciences of the United States of America,* 95**,** 14932-7.
728 WILLIAMS, G. H., SWINN, R., PREVOST, A. T., DE CLIVE-LOWE, P., HALSALL, I., GOING, J. J.,
729 HALES, C. N., STOEBER, K. & MIDDLETON, S. J. 2004. Diagnosis of oesophageal cancer
730 by detection of minichromosome maintenance 5 protein in gastric aspirates. *British*
731 *journal of cancer,* 91**,** 714-9.
732 YIN, X., FARIN, H. F., VAN ES, J. H., CLEVERS, H., LANGER, R. & KARP, J. M. 2014. Niche-
733 independent high-purity cultures of Lgr5+ intestinal stem cells and their progeny.
734 *Nature methods,* 11**,** 106-12.

735

736

737

738 **Figure Legends**

739 **Figure 1. Mcm2 is expressed ubiquitously along the crypt-villus axis and declines slowly as**
740 **cells differentiate**

741 (**A**) Sections of normal human (top panel) and mouse (bottom panel) small-intestine were
742 stained with Phalloidin (Green) and an antibody against Mcm2 (Red). Scale bars: 200 μm.

743 (**B**) Mean Mcm2 intensities for segmented nuclei were plotted along the crypt-villus axis for
744 mouse and human tissue. Location of the crypt and villus domains is indicated.

745 (**C**) An intestinal crypt stained with Hoechst (Blue), Phalloidin (Green) and an antibody
746 against Mcm2 (Red). Individual cells in interphase and mitosis (metaphase and cytokinesis)
747 are outlined by dashed white lines.
748
749 (**D**) Images of Lgr5-GFP stem cells (Green) (top panel) co-stained with a Mcm2 antibody
750 (Red). The correlation (Pearson's correlation R=0.81, p<0.0001) between mean Mcm2 and
751 Lgr5-GFP intensities for 69 Lgr5-GFP(+) cells normalised to the maximum intensity for an
752 individual crypt is shown.

753 (**E**) Images of UEA(+) Paneth Cells (top panels) co-stained with an Mcm2 antibody (Red) and
754 UEA (Green). Mean Mcm2 intensity for segmented nuclei of UEA(+) Paneth cells was
755 compared with interphase cells (Right panels).

756 (**F**) Mcm2 (Green) and UEA (Red) expression in subsets of UEA(+) cells in crypt and villus
757 domains. UEA(+) cells at the crypt base represent Paneth cells.

758 (**G**) Quantification of mean Mcm2 intensity in individual UEA(+) cell populations. UEA(+) cells
759 in the crypt base (Paneth cells, N=224), in the upper crypt compartment (Crypt, N = 132) and
760 in the villus compartment (Villus, N = 225) were identified manually, and the nuclear Mcm2
761 intensity was determined for individual cells (All cells, N = 33,736). There was a significant
762 difference between UEA(+) cells in the crypt and villus compartments (T test, p<0.0001)

763

Figure 2. Visualising Mcm2 licensing in intestinal crypts

(**A**) Representative bright-field images of extracted and unextracted isolated intestinal crypts. Scale bar: 90 µm

(**B**) Representative images of isolated crypts stained with antibodies against Mcm2 (Red) or Ki67 (Purple). Scale bar: 10 µm

(**C**) The Mcm2 labelling index for unextracted and extracted crypts is significantly different (Mean +/- SEM, N=10 crypts (T test, $p<0.0001$).

(**D**) Representative intestinal crypts stained with Hoechst (Blue) and antibodies against Mcm2 (Red) and phospho-histone H3 (pH-H3) (Green).

(**E**) Representative flow cytometry profiles for extracted and unextracted isolated crypt epithelial cells showing Mcm2 vs. DNA content.

(**E'**) Suggested model of the licensing profile shown in panel E. Deeply quiescent cells, do not express Mcm2 and have a very low Mcm2 signal. Cells expressing only soluble Mcm2 (G_0/ G_1) show a similar Mcm2 signal to G_2 cells. After a proliferative fate decision has been made, cells license and become committed to S-phase entry. Cells enter S-phase after maximal origin licensing (Active-G_1). During S-phase, Mcms are then displaced from DNA during replication.

(**F**) Representative images of extracted and unextracted intestinal organoids stained with an antibody against Mcm2 (Red).

(**G**) The Mcm2 labelling index for unextracted and extracted organoids. Data is displayed as Mean +/- SEM, N = 3 organoids and shows a significant difference (T test, $p<0.0001$).

Figure 3. The licensing state defines distinct proliferative zones in intestinal crypts

(**A**) Representative image of an extracted intestinal crypt isolated after a 1 hour EdU pulse *in vivo* (EdU, Green) and stained with Hoechst (Blue) and antibodies against Mcm2 (Red) and pH-H3 (White). Co-staining shows distinct cell-cycle phases (bottom panels): Licensed cells committed in G_1 (Mcm2(+), EdU(-)); Early (Mcm2(+), EdU(+)) to Late (Mcm2(-), EdU(+)) S-phase), and mitotic cells (pH-H3(+)). Negative cells represent deeply quiescent (G_0), terminally differentiated cells or cells in G_1, which have not made a proliferative fate decision, remaining unlicensed. The crypt base is to the left of the displayed image.

(**B**) Nuclear volume was estimated in cells at the distinct cell-cycle phases identified previously: Negative ($G_0/G_1/G_2$: N =115), G_1 Licensed (Mcm(+), EdU(-): N=38), S-phase (Mcm(+), EdU(+): N=24) and Late-S/G_2 (Mcm(-), EdU(+): N=26). Top Panels show representative examples of each cell-cycle phase and the associated 3D rendered nuclei. There was a significant difference in the size of Licensed G_1, S and Late-S/G_2 nuclei (T test, $p<0.0001$).

(**C**) Representative images of intestinal crypts isolated after a 1 hour EdU pulse (Green) *in vivo*. Displayed are 3D projections of extracted and unextracted crypts stained with Hoechst (Blue) and an antibody against Mcm2 (Red).

(**D**) Comparison between cells expressing Mcm2 protein and DNA-bound Mcm2 along the crypt-villus axis between unextracted (N=101 crypts) and extracted (N=109 crypts) (taken from 3 mice). Data is displayed as the mean % of cells per set distance bin.

(**E**) All cells were divided into 4 distinct groups based on Mcm2 and EdU intensities. These groups represent distinctive cell-cycle phases as defined by their total (unextracted N=101 crypts) or licensed (extracted N=109 crypts) Mcm2 content: **Extracted:** 1) **Unlicensed** (Mcm2(-), EdU(-)), 2) **G_1 licensed** (Mcm2(+), EdU(-)), 3) **Early/Mid S-phase** (Mcm2(+), EdU(+)) and 4) **Late-S/G_2** (Mcm2(-), EdU (+)). The data is represented as the population mean of the total cells per distance bin, Mean +/- SEM.

(**F**) The distance of the most distal Mcm2(+) and EdU(+) cells to the crypt base was compared in extracted and unextracted crypts. Data was scored manually for 10 representative crypts per condition. Licensed cells (Mcm2(+)) were significantly closer to the crypt base than EdU(+) cells (T test, $p=0.0015$. Cells expressing Mcm2 protein extended significantly above the last EdU(+) cell (T test, $p<0.0003$)

(**G**) Representative images of crypts isolated 17 hours after administration of EdU (Green). 3D projections of extracted and unextracted crypts stained with Hoechst (Blue) and an antibody against Mcm2 (Red) are shown.

(**H**) Cells were divided into 4 distinct groups as in Panel **E** (N=51 Crypts).

Figure 4. Intestinal stem cells reside in an unlicensed shallow' G_0

(**A**) Representative image of an extracted crypt base isolated 1 hour after a pulse of EdU (Green) and stained with Hoechst (Blue), UEA (Red) and antibodies against Mcm2 (White). Nuclear morphology and UEA signal were used to distinguish between UEA(+) Paneth Cells (Dashed outline, blue stars) and UEA(-) stem cells (Red stars).

(**B**) The average % of UEA(-) stem cells that fall into the previously defined cell-cycle bins: (Negative $G_0/G_1/G_2$; G_1 licensed; S-phase; S/G_2 phase; N=68 crypts).

(**C**) Representative flow cytometry profiles of (**i**) isolated $Lgr5^{Hi}$ intestinal stem cells showing DNA-bound Mcm2 and DNA content (2ndry only control samples are shown); (**ii**) cells with a 2N (G_1) DNA content were selected and the DNA-bound Mcm2 is shown (left panels); their Ki67 staining was then compared (right panels). (iii) The frequency distribution of mean DNA-bound Mcm2 intensities for Mcm2(+) cells in G_1 cells is displayed. Hypothetical scenarios for model frequency distributions of 'fast', 'slow' and 'no' licensing are displayed. The profile for intestinal stem-cells is most similar to a 'no loading' scenario.

(**D**) Comparison of DNA-bound Mcm2 content of Lgr5(+) and Lgr5(-) G_1 cells and of cells in very early S-phase.

(**E**) Label retaining '+4' cells were visualised using a pulse-chase protocol in H2B-GFP mice (Supplementary Figure 4). A representative image of a crypt base is displayed highlighting a label retaining (+4) cell (white arrow) that is GFP(+) UEA(-), and is distinct from label retaining Paneth cells (GFP(+), UEA(+)).

(F) Representative images of H2B-GFP label-retaining cells in extracted intestinal crypts stained with Hoechst (Blue) and an antibody against Mcm2 (Red). $H2B\text{-}GFP^{Hi}$ cells (bright Green) represent Paneth cells and +4 cells, and $H2B\text{-}GFP^{Low}$ cells (Faint Green) represent daughter cells that have diluted H2B-GFP content as a result of cell division.

(**G**) Quantification of the mean DNA-bound Mcm2 intensities in GFP^{Hi} label retaining (LR) and GFP^{low} daughter cells compared with the total cell population (all cells). Displayed are the mean +/- SEM (N=20 crypts).

Figure 5. Contribution of the stem-cell niche to cell-cycle dynamics

(**A**) Representative image of an extracted intestinal organoid stained with Hoechst (Blue), Phalloidin (Green) and an antibody against Mcm2 (Red).

(**B**) Representative flow cytometry profiles from cells isolated from organoids (left) or from intestinal tissue (right). Displayed is the quantification of DNA-bound Mcm2 content of G_1 cells (**i**). The percentage of fully licensed cells is also shown. The frequency distribution (ii) of mean DNA-bound Mcm2 intensities for Mcm2(+) cells within G_1 cells for organoids and intestinal crypts are displayed.

(**C**) Representative flow cytometry profiles of isolated organoid epithelial cells quantifying Ki67 (**i**) and DNA-bound Mcm2 (**ii**) against DNA content or the comparison of DNA-bound Mcm2 vs Ki67 (**iii**) Displayed is a representative plot from organoids grown in ENR media alongside epithelial cells from isolated crypts (iv) (**See also S5 Figure A**).

(**D**) Representative flow cytometry profiles of isolated organoid epithelial cells grown in ENR (control) and treated with the EGFR inhibitor Gefitinib, for the indicated times (**i-iii**). After 4 Days in Gefitinib, organoids were reactivated by removal of the Gefitinib and re-addition of fresh growth factors for 2 days (**iv**). Displayed are profiles comparing DNA-bound Mcm2 vs Ki67 (Top panels) or total Mcm2 content (Bottom panels).

(**E**) Representative flow cytometry profiles of isolated organoid epithelial cells grown in ENR or ENR-CV media for 6 days comparing DNA-bound Mcm2 vs Ki67 content.

(**F**) Representative flow cytometry profiles from extracted cells isolated from organoids treated with ENR or ENR-CV for indicated time periods. Displayed is the comparison of DNA-bound Mcm2 vs Ki67 content.

(**G**) Organoids in ENR-CV media were treated with Gefitinib (EGFi) for 1 day and were 're-activated' by fresh addition of ENR-CV for a further day. Representative flow cytometry profiles of isolated organoid epithelial cells are shown comparing DNA-bound Mcm2 vs Ki67 content.

Figure 6. Model of Origin licensing dynamics in intestinal epithelial cells

In a normal cell-cycle, Mcms are expressed ubiquitously in all stages. The licensing of DNA with MCM2-7 occurs in late M and throughout G_1, when a cell receives a stimulus to commit to the cell cycle. As DNA is replicated during S-phase, MCM2-7s are displaced from DNA and are prevented from relicensing in G_2. During terminal differentiation, MCM2-7 are not actively transcribed and the proteins are gradually lost in post-mitotic cells. However, after the final mitotic division, cells make a binary decision never to license their DNA, even though the protein is still present. Mcm proteins then degrade slowly, where cells enter a terminally differentiated state (deep G_0). Alternatively, cells can exit mitosis, not relicense their DNA but maintain proliferative markers and disengage from the cell cycle for some time (shallow G_0). Two major classes of intestinal stem cells exist: 'Active' stem cells, engaged with the cell-cycle, and reserve, quiescent Label Retaining Cells. Label retaining cells are in a state of 'deep' quiescence, and do not contain MCM2-7 because they have disengaged from the cell cycle for some time. In this study, we show that most 'Active' Lgr5(+) stem cells reside in an unlicensed state, but contain MCM2-7 proteins. These cells reside in a shallow-G_0' until they make a proliferative fate decision, enter the cell-cycle and license. This provides an explanation for the elongated cell-cycle of Intestinal stem cells: They reside in a partial resting state where they may be able to respond to niche cues to divide. This therefore may constitute a unique mechanism to control stem cell numbers.

Supplementary Figure Legends

S1 Figure. Image analysis

(**A**) Maximum intensity projections of intestinal tissue revealing intestinal crypts and villi (left panels). Individual X-Y sections are also shown to reveal the epithelium (right panels). Tissue was stained with Phalloidin (Green) and Hoechst (Blue) and an antibody against Mcm2 (Red).

(**B**) Image analysis work-flow.

(**C**) Representative image of an extracted isolated crypt 1 hour after an EdU pulse (Green) stained with Hoechst (Blue) and an antibody against Mcm2 (Red).

(**D**) Detection of nuclei in the crypt in panel A in 3D. Nuclei were detected in 3D using segmentation tools in Imaris. Detection was validated visually or each individual crypt.

(**E**) Segmentation of the region of interest defined by nuclei detection in panel B.

(**F**) A distance transform was performed in Imaris to measure the distance of each nucleus to a reference nucleus at the crypt base. Visual representations of distances divided into different bins are displayed (Green, 0-10µm; Yellow, 10-20 µm; Red, 20-30µm; Blue, 30-40µm; Magenta, 40-50µm).

(**G**) Representative 3D quantification of the crypt in panel A shows the distance from the crypt base (X-axis), DNA-bound Mcm2 (Y-axis) and EdU incorporation (Z-axis).

(**G**) Quantification of Mcm2 and EdU intensities in cell-cycle phases shown in Figure 3A. Displayed are the mean intensities for DNA-bound Mcm2 and EdU for each cell-cycle phase (N=10 cells).

S2 Figure. Clonal cell-cycle patterns in the intestinal epithelium

(A) Representative section through an extracted crypt after a 1 hour EdU pulse (Green) and stained with Hoechst (Blue) and an antibody against Mcm2 (Red). Discrimination of cell-cycle staging using DNA-bound Mcm2 and EdU incorporation patterns allows visualisation of clonal cell-cycle field effects revealing many neighbouring cells with similar DNA-bound Mcm2 and DNA replication patterns. These clones may represent lineages of from single cells that progress through the cell cycle at the same rate.

(**B**) Representative image of an isolated crypt in which surface rendering was performed on all nuclei and colour codes applied to reflect cell-cycle stage. Representative cell-cycle distributions for isolated Ki67(+), Lgr5(+) and Lgr5(-) intestinal epithelial cells are shown.

(**C**) Representative cell-cycle distributions for isolated Ki67(+), Lgr5(+) and Lgr5(-) intestinal epithelial cells. The average of each cell-cycle phase is displayed for duplicate isolations.

(**D**) Nuclear volumes were rendered for individual nuclei in whole intestinal crypts isolated 1 hour after labelling with EdU. Image shows nuclei (Blue), EdU (Green) and licensed Mcm2 (Red). Maximum intensity projections of the original image are displayed at the top and corresponding rendered nuclei at the bottom. Nuclear surfaces were colour-coded according to cell-cycle states: Blue, unlicensed; Red, Licensed G_1; Yellow, S-phase; Green, Late-S/G_2. Nuclear volumes were measured for all nuclei in representative crypts (N=3). Unlicensed (N=368); G_1 (N=104); S-phase (N=41); Late-S/G_2 (N=70) and the distance of cells from the crypt base were binned into 10μm intervals. Known parameters of the nuclear volume for known cell-cycle stages (Figure 3B) are overlaid.

S3 Figure. Ki67 expression along the crypt-villus axis

(**A**) A representative isolated crypt 1 hour after labelling with EdU (Green) and stained with an antibody against Ki67 (magenta)

(**B**) Quantification of the distribution of Ki67(+) cells along the crypt axis. Cells were binned into four groups: Negative (Ki67(-), EdU(-)); Ki67(+), EdU(-); Ki67(+), EdU(+) and Ki67(-), (EdU(+) and by their distance from the crypt base. Data is displayed as the average percentage of a particular cell subtype, per distance bin. Data is displayed as Mean +/- SEM. Data from 75 crypts is displayed, N = 14,264 cells.

S4 Figure. H2B-GFP labelling strategy

(**A**) Labelling strategy. H2B-GFP expression was induced in all intestinal epithelial cells in H2B-GFP mice by administration of doxycycline for 7 days. After complete labelling, doxycycline was removed and mice rested for 4-7 days. During this chase period, the majority of H2B-GFP(+) cells are lost by label dilution due to cell division and upward migration.

(**B**) Representative images of whole-mount sections of H2B-GFP expressing small-intestinal tissue after a 7day labelling period. Maximum intensity images show fully labelled crypts and villi.

(**C**) A representative image of an isolated villus fragment isolated 7 days after last doxycyclin administration, stained with Hoechst (Blue) and an antibody against GFP (Red). Image shows the accumulation of GFP(+) label retaining cells at the villus tip.

(**D**) A vibratome section of H2B-GFP epithelium after a 7-day chase period. Tissue was stained with Hoechst (Blue) and an antibody against GFP (Red). The unamplified GFP signal (white) is only detectable in infrequently dividing cells such as Paneth cells or label retaining +4 cells. Antibody-mediated amplification of the GFP signal allows visualisation of lower GFP expression in daughter cells persisting in the crypt.

(**E**) Quantification of the mean GFP intensity for all cells along the crypt-villus axis 7 days after final doxycycline treatment. The majority of GFP(+) cells reside within the stem cell compartment 0-40µm from the crypt base.

(**F**) Extraction does not affect H2B-GFP expression. Representative image of a fully induced, extracted H2B-GFP (Green) crypt stained with an antibody against Mcm2 (Red).

S5 Figure. Manipulation of the stem cell niche can artificially induce shallow-G_0

(**A**) Representative flow cytometry profile of extracted epithelial cells isolated from organoids in ENR media. The displayed image is the same profile displayed in Figure 5C. The populations in boxed regions 1-7 are overlaid onto the Mcm2 and Ki67 cell-cycle profiles.

(**B**) Representative images of Lgr5-GFP organoids treated with ENR or ENR-CV. In ENR-CV treated organoids, the majority of cells express Lgr5.

(**C**) Representative flow cytometry profiles from extracted cells isolated from organoids treated with Valproic acid or Chir99021 alone for indicated time intervals.

(**D**) Representative flow cytometry profiles from extracted cells isolated from organoids treated with DAPT for indicated time intervals.

(**E**) Model for the unique cell-cycle characteristics of organoid epithelial cells.
Normal, highly proliferative cells, express Ki67 and Mcm2 protein that is not DNA-bound (**1**). During a normal cell-cycle, cells are activated from this shallow-G_0 state, and rapidly license origins (**2**). Mcms are subsequently displaced during DNA replication (**3**) and remain unlicensed through G_2 (**3**). Inhibiting EGFR causes highly proliferative cells ($Ki67^{hi}$) to arrest in shallow-G_0 with maintained Mcm2 protein expression. Prolonged EGFRi treatment causes transition into an intermediate state of G_0 accompanied by loss of Ki67 expression ($Ki67^{lo}$), but maintenance of MCM2-7 protein expression (**4**). Induction of terminal differentiation by inhibition of Notch signalling is associated with a terminal loss of MCM2-7 proteins, and entry into deep-G_0 (**5**). HDAC inhibition (HDACi) or Notch activation induces a unique subset of $Ki67^{lo}$ shallow-G_0 cells to license origins independently of Ki67 expression (**6**). We suggest that the unique cell population observed upon ENR-CV / ENR-V treatment may be a reserve subset of stem cells that express Lgr5 and start expressing MCM2-7 and enter shallow-G_0 from deep-G_0. These cells have unique cell cycle characteristics, and can immediately license origins independently of Ki67 expression (6→2→3).

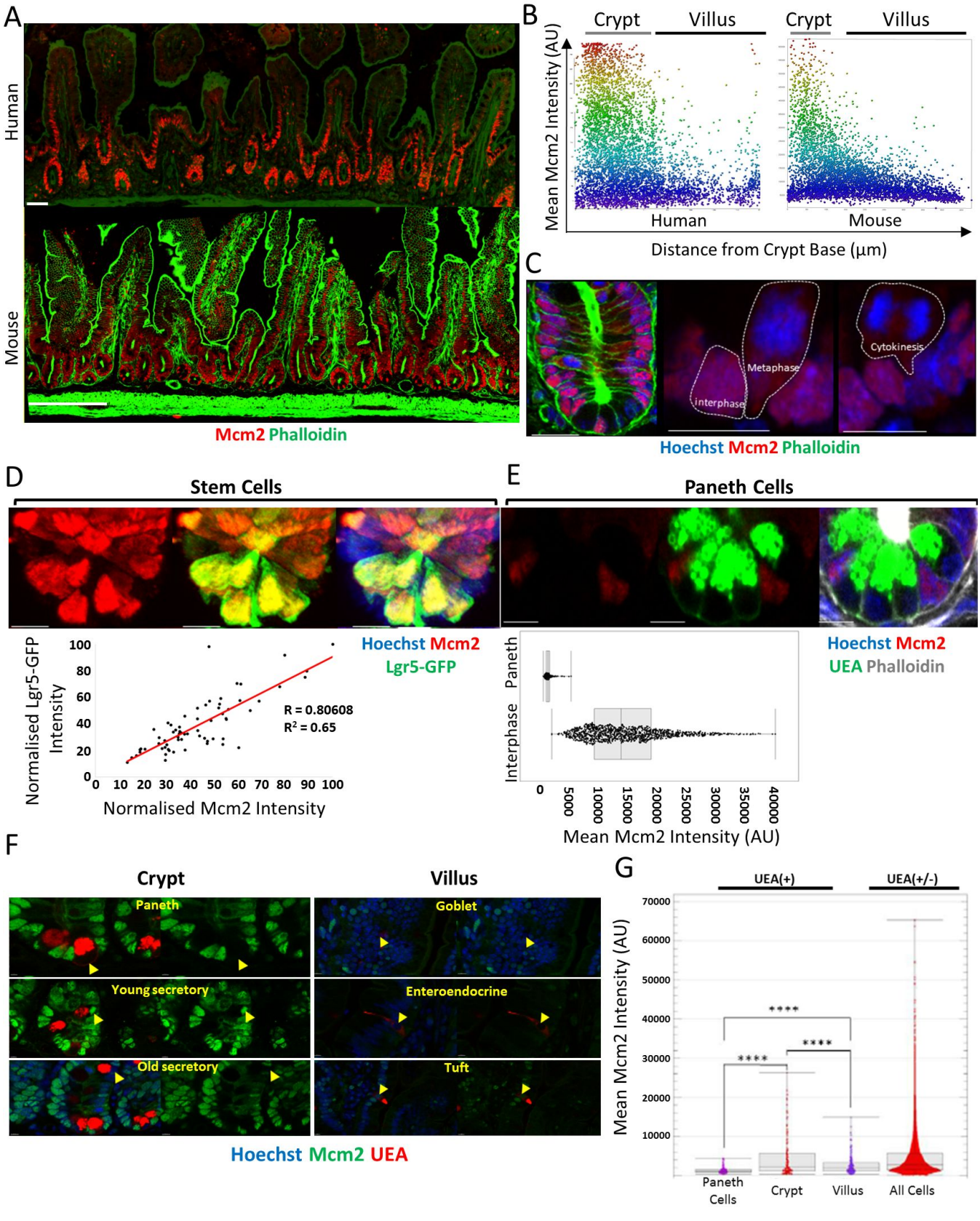

Carroll et al., Figure 1

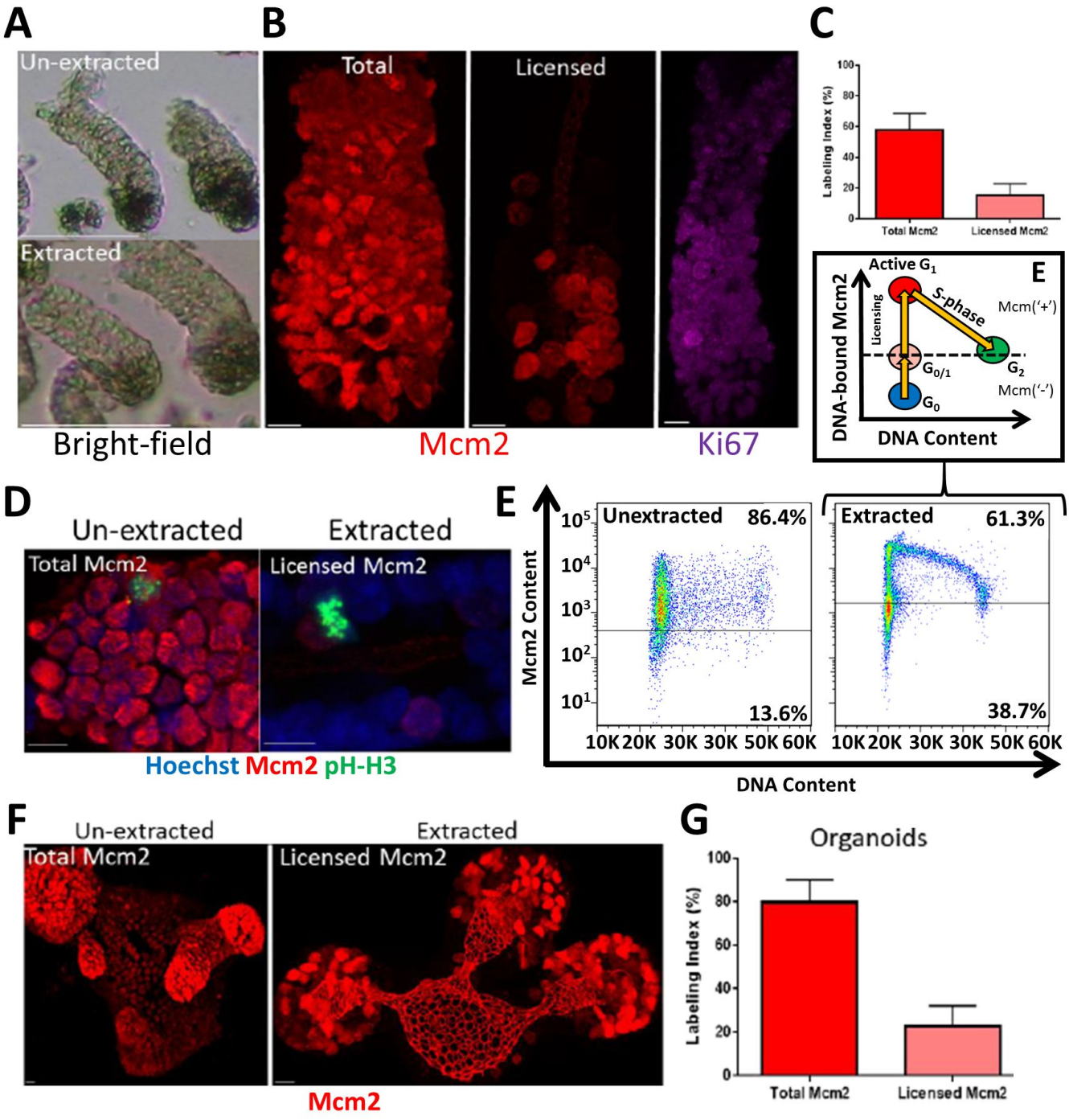

Carroll et al., Figure 2

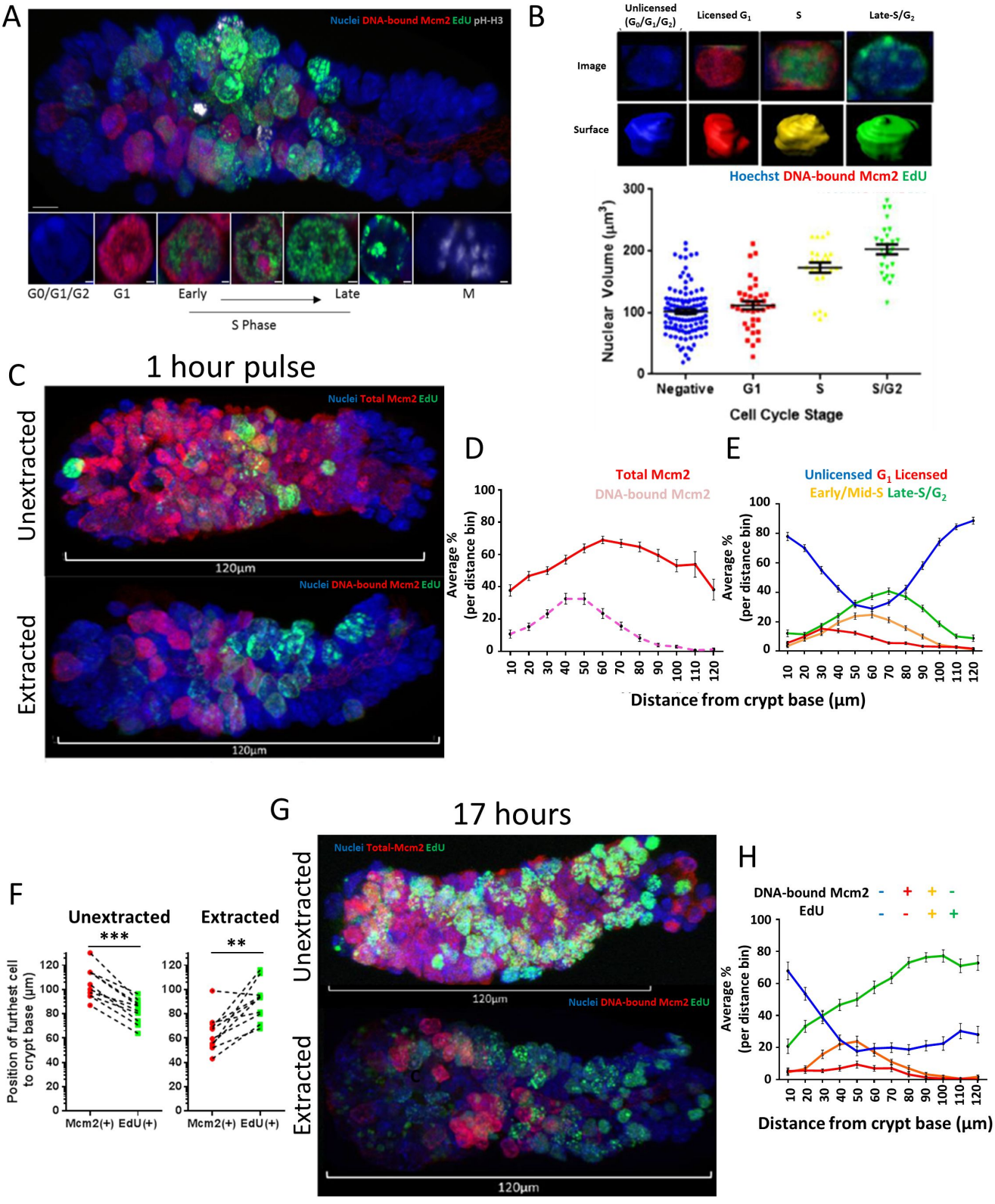

Carroll et al., Figure 3

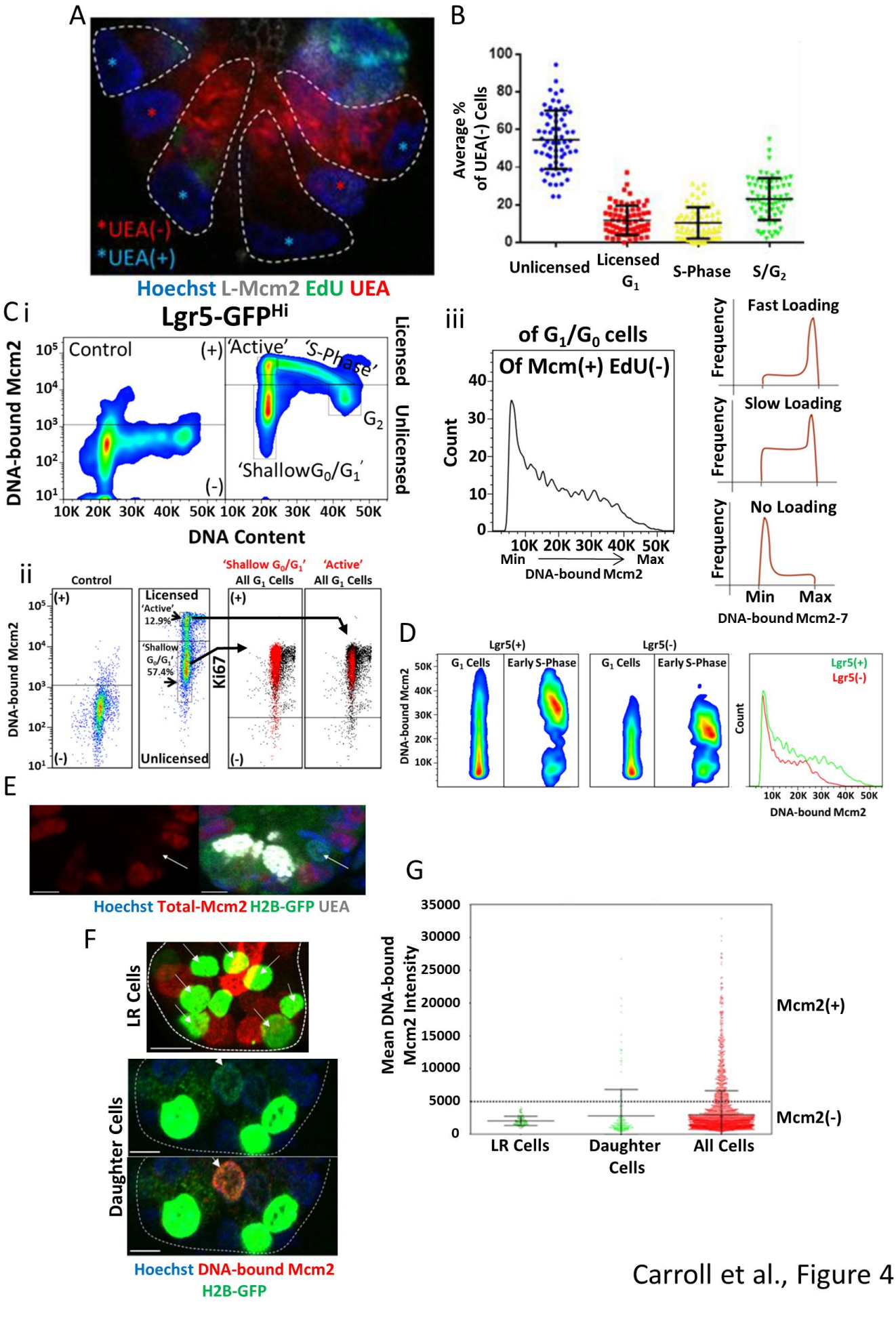

Carroll et al., Figure 4

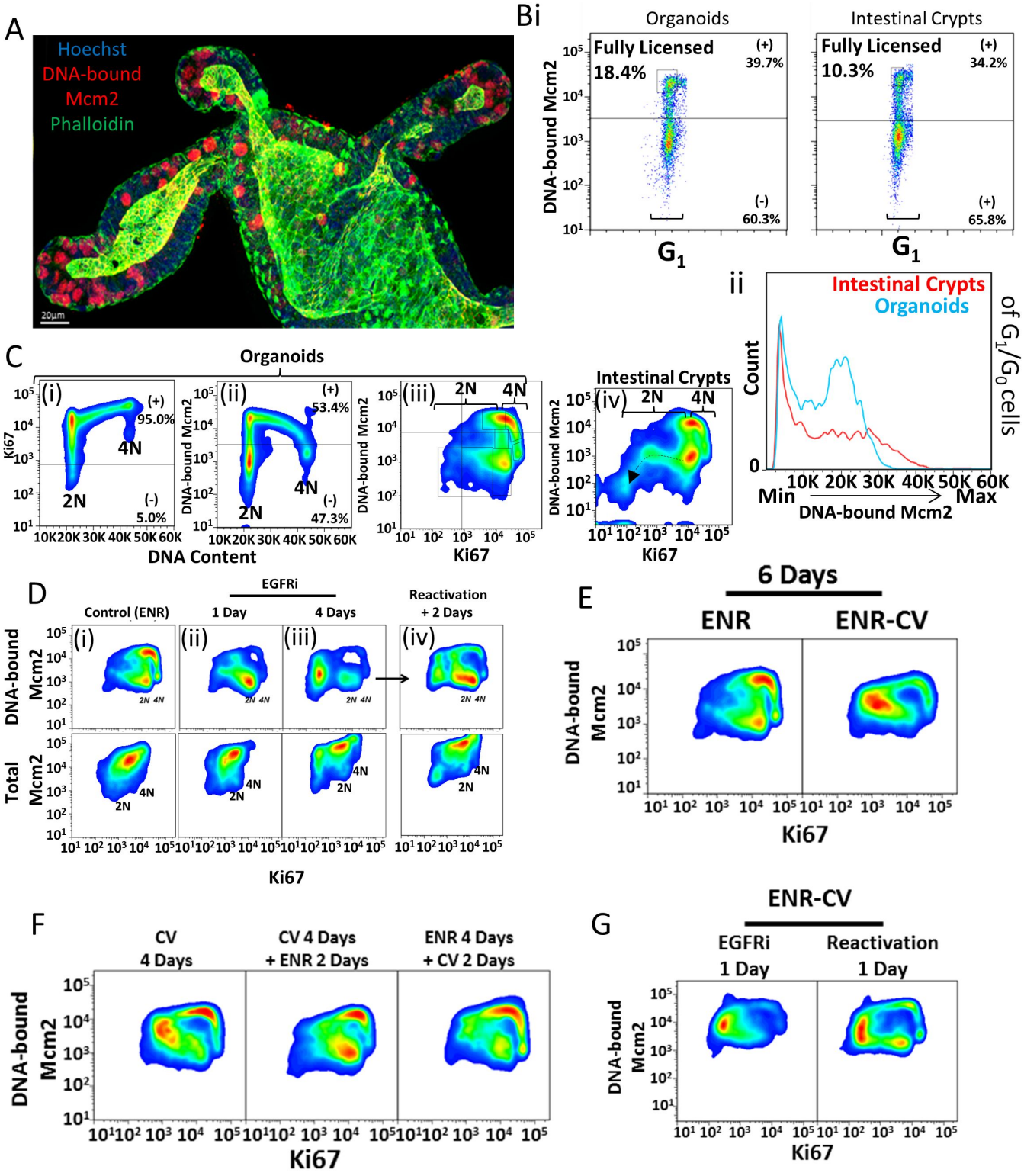

Carroll et al., Figure 5

Carroll et al., Figure 6

Mcm2-7 Protein [redacted]

+4 LRC
Paneth
Lgr5

Stem-cell Compartment
Transit-amplifying Compartment
Terminal Differentiation

'Deep' G_0

Shallow G_0

Lgr5(+) Stem Cell
'+4' Stem Cell
'Active'
Shallow G_0
Deep G_0

M
G_1
S
G_2

free Mcm2-7 hexamers
Mcm2-7 on DNA
active helicase

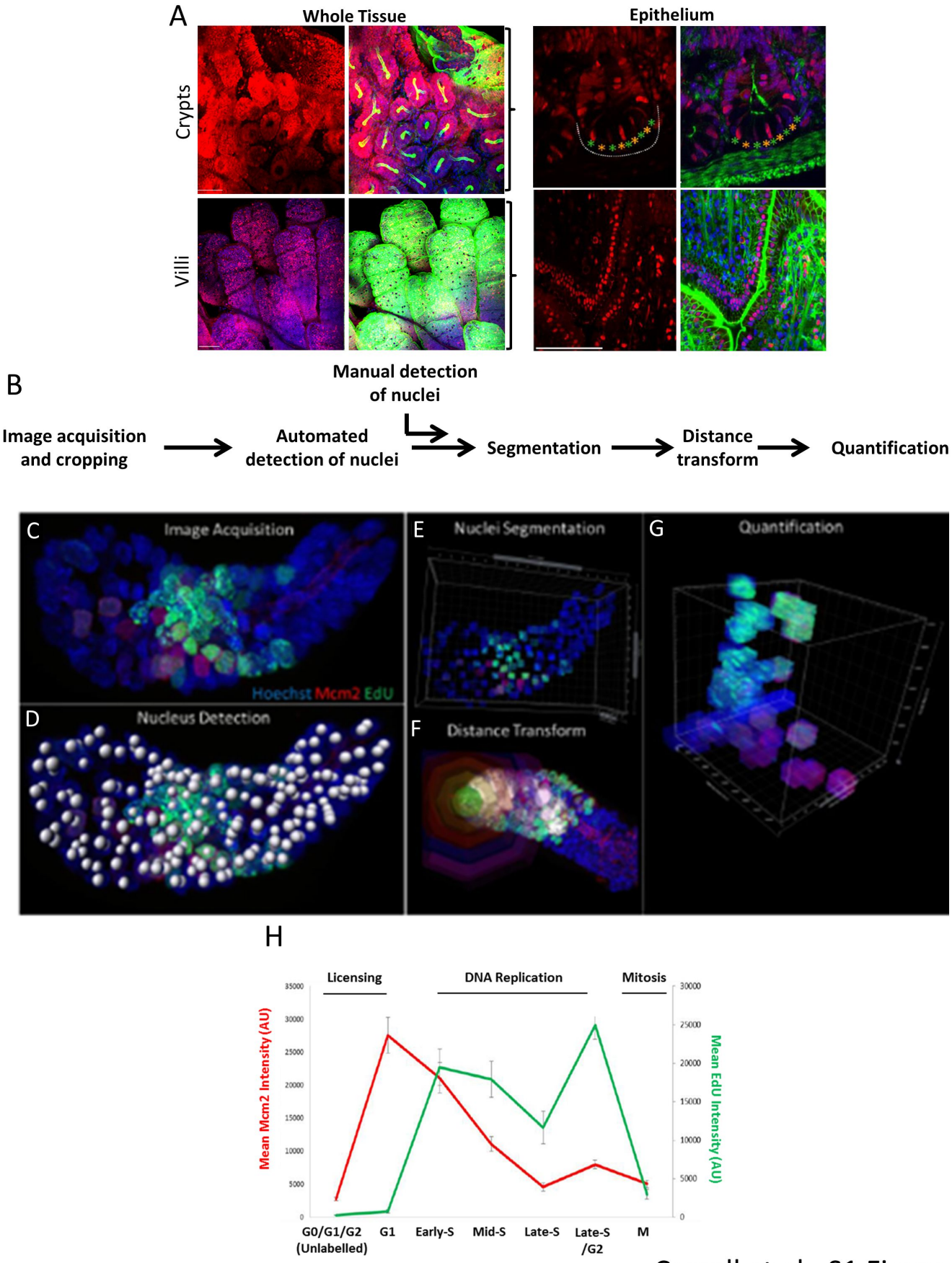

Carroll et al., S1 Figure

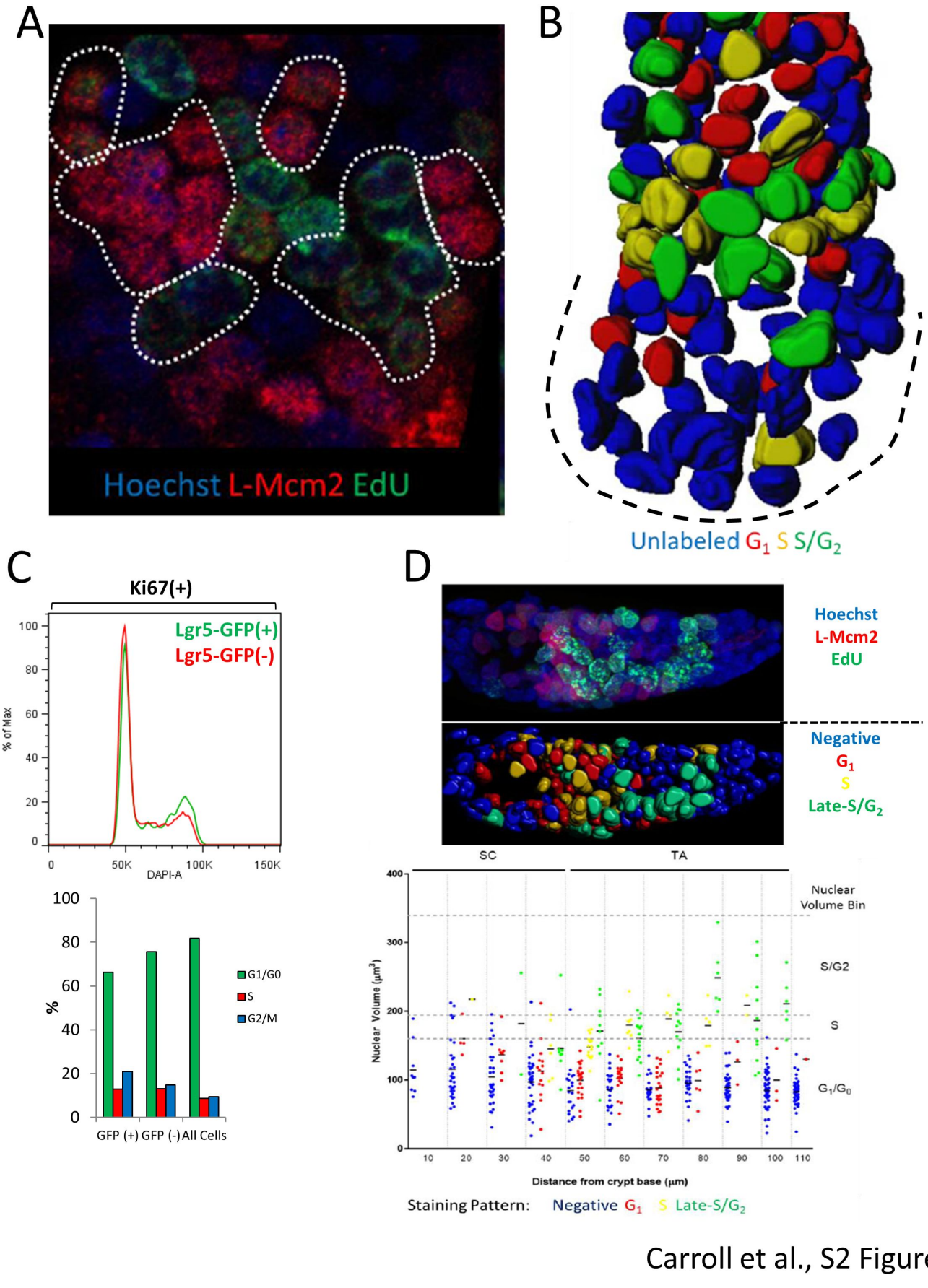

Carroll et al., S2 Figure

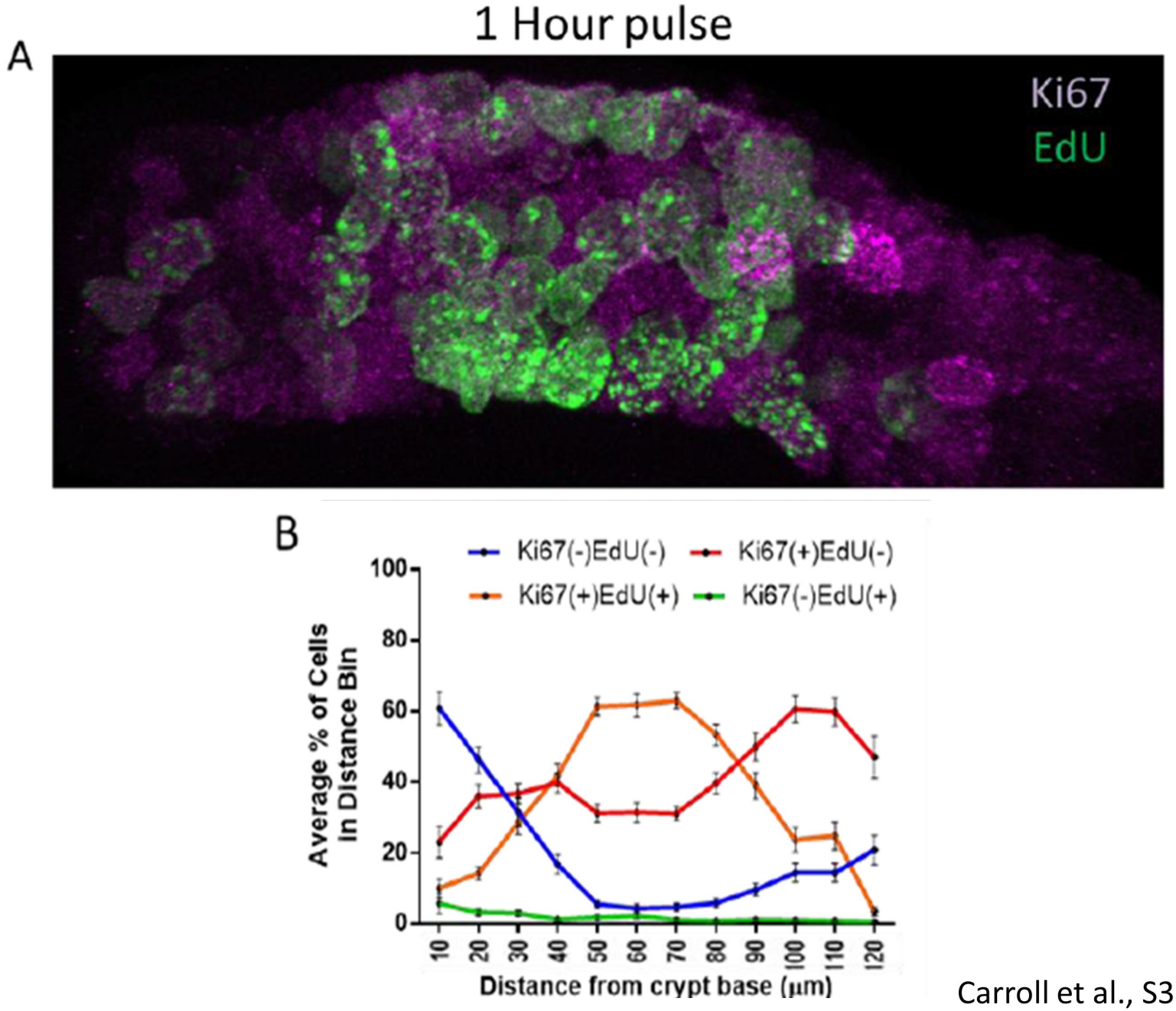

Carroll et al., S3 Figure

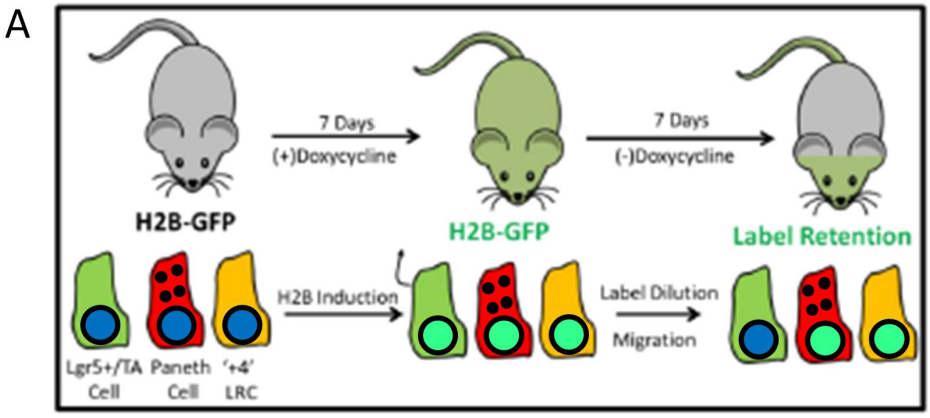

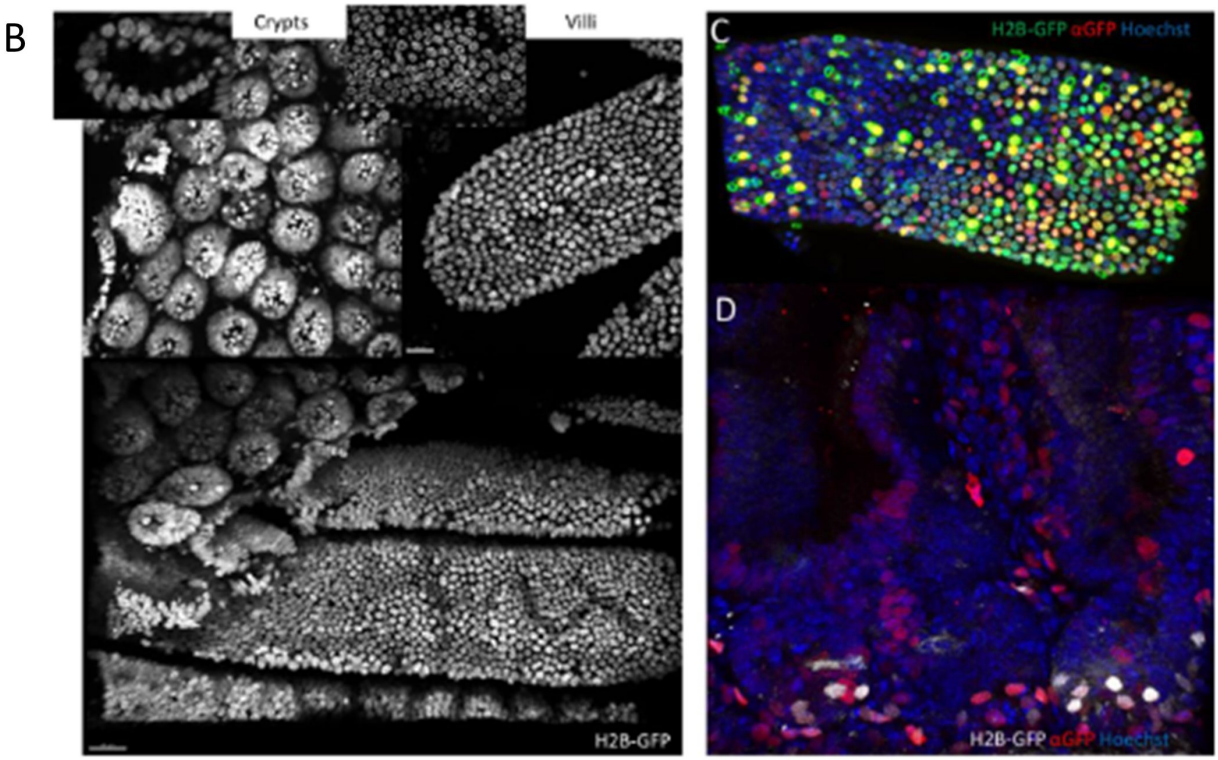

7 Days Induction

7 Days Chase

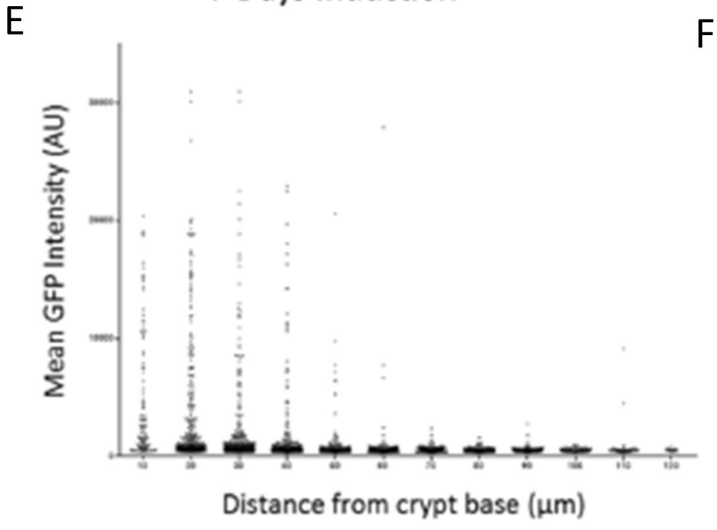

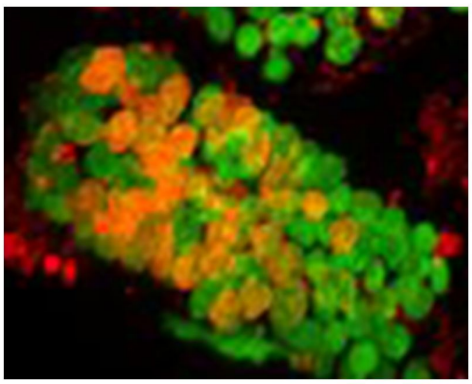

DNA-bound Mcm2 H2B-GFP

Carroll et al., S4 Figure

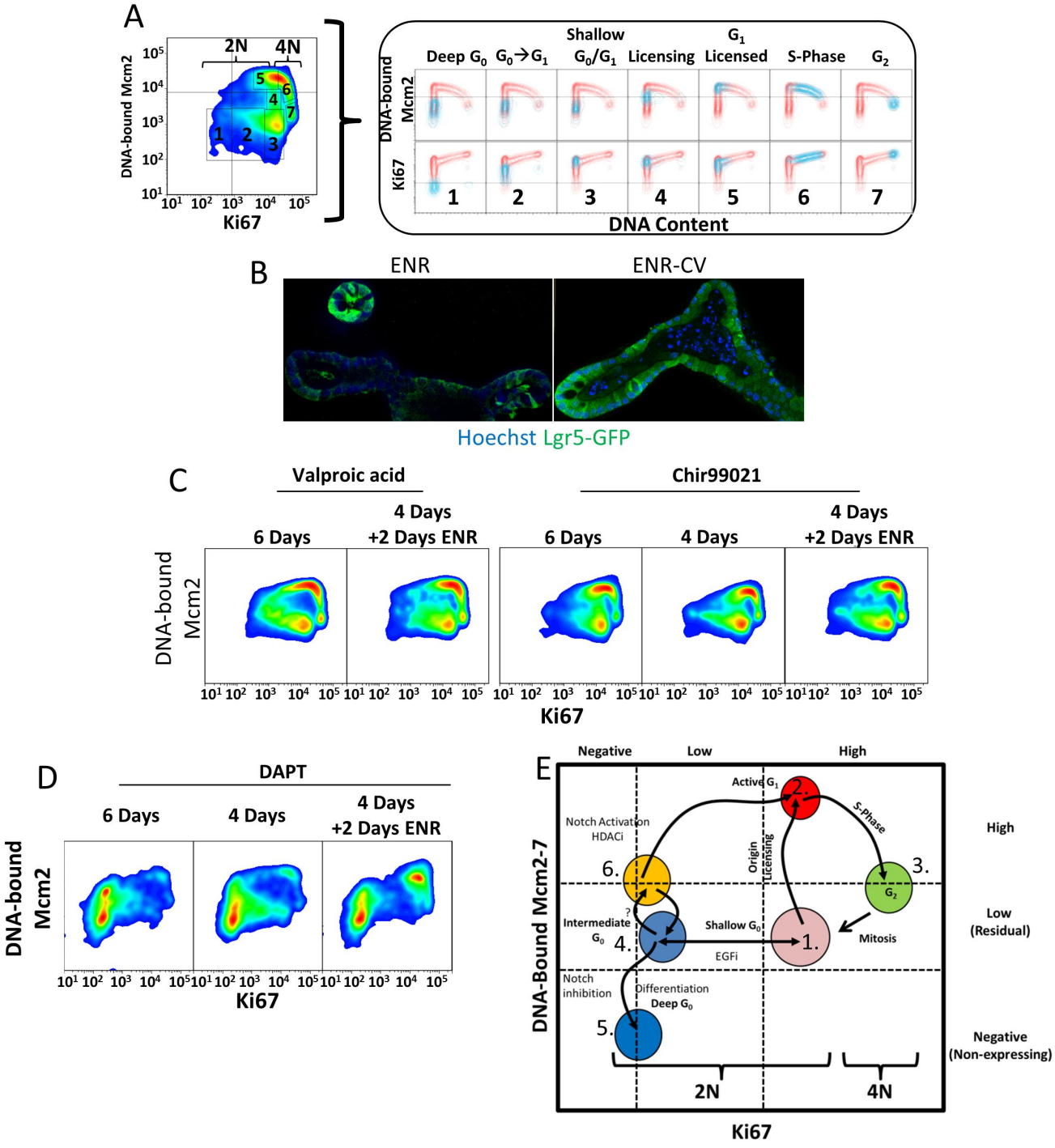

Carroll et al., S5 Figure